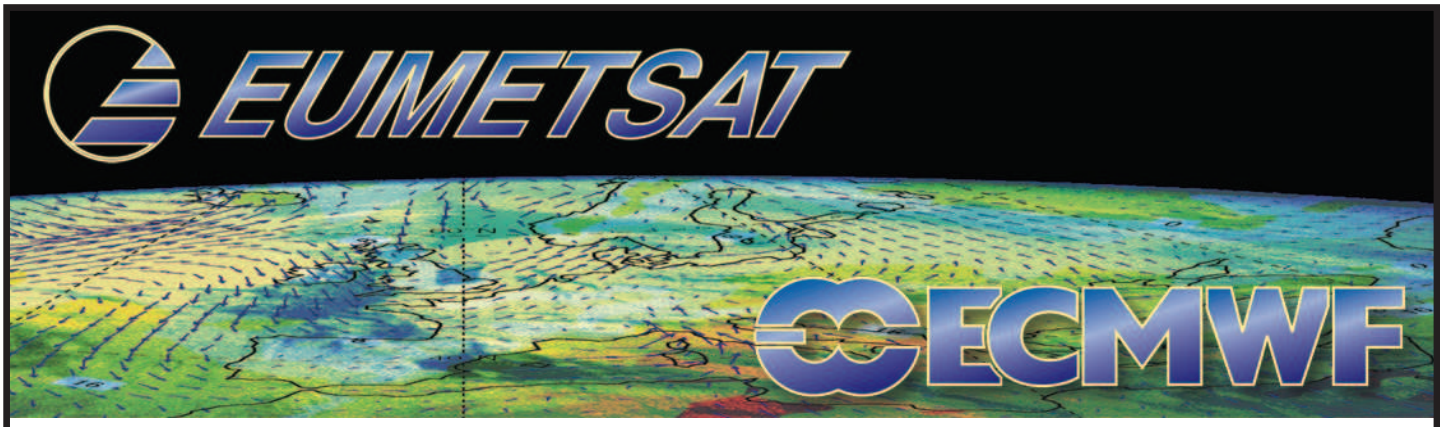

EUMETSAT/ECMWF Fellowship Programme
Research Report No. 24

Assimilating AMSU-A temperature sounding channels in the presence of cloud and precipitation

Alan J. Geer, Peter Bauer and
Stephen J. English

Simultaneously released as ECMWF technical memorandum 670

April 2012

Series: EUMETSAT/ECMWF Fellowship Programme Research Reports

A full list of ECMWF Publications can be found on our web site under:
http://www.ecmwf.int/publications/

Contact: library@ecmwf.int

European Centre for Medium Range Weather Forecasts
Shinfield Park, Reading, RG2 9AX, England

Abstract

A better assimilation of satellite radiances in cloudy and precipitating areas should help improve forecasts by (i) providing greater coverage of temperature and humidity in meteorologically active areas and (ii) directly constraining cloud and precipitation. Advanced Microwave Sounding Unit A (AMSU-A) is used for sensing atmospheric temperature and is one of the most important sensors in the global observing system, yet at ECMWF, except for a simple cloud-screening, it is still assimilated without considering the effect of cloud or precipitation. There may be benefits in using the 'all-sky' approach, which is already operational for microwave imagers. To extend this to AMSU-A requires a model for observation error that prescribes larger errors in cloudy and precipitating regions than in clear skies, and larger errors at nadir where the weighting function sees deepest into the atmosphere.

This study focuses on channels 4 and 5 of AMSU-A, which are intended for lower and mid-tropospheric temperature sounding, but are also sensitive to hydrometeors and the surface. Channel 4 is not yet assimilated operationally. In the full observing system, the incremental impact of all-sky AMSU-A channel 4 from two satellites is similar to that of adding another microwave imager; in other words it brings new information on water vapour and cloud, but has little impact on temperature. It is likely that other observations, such as infrared sounder radiances, already constrain the lower tropospheric temperature quite well. A first implementation of all-sky assimilation of channel 5 was unable to replicate the quality of the existing clear-sky assimilation. Mainly this was due to an imperfect experimental setup that allowed changes in the number of observations, the screening and the prescribed observation error. With more development it should be possible to match the quality of the existing technique, but it may be hard to improve on clear-sky assimilation. This is because: (i) All-sky assimilation can reduce the constraint on temperature by allowing increments to go into the cloud fields; (ii) Clear-sky channel 5 assimilation already has an 80% coverage over ocean, so there is limited scope to extend the coverage further; (iii) Ignoring the presence of liquid water cloud appears to be a minor part of the error budget for clear-sky channel 5 assimilation; (iv) The 'double-penalty' problem can increase the error budget in all-sky assimilation (compared to clear-sky), particularly in the tropics; (v) The all-sky technique suffers ongoing issues with water vapour and temperature spinup in the tropics, likely to do with the data assimilation and the water vapour control variable. Nevertheless, development will continue.

1 Introduction

Temperature-sensitive microwave radiances from Advanced Microwave Sounding Unit A (AMSU-A) and its predecessor MSU have been one of the most important parts of the global observing system for many years (e.g. Derber and Wu, 1998; English et al., 2000). This remains true even after the introduction of hyperspectral infrared sounders (e.g. Cardinali and Prates, 2011). When ECMWF reduced the observation error assigned to AMSU-A temperature channels there was a 2% improvement in forecast scores (Bormann et al., 2011b) and this was one of the most significant operational upgrades of recent years. However, AMSU-A is still assimilated without considering the effect of cloud or precipitation, and cloud-affected observations are rejected (Bormann, 2008). This work examines whether the cloud and precipitation aspects could be dealt with better.

At ECMWF, microwave imagers are now assimilated using an all-sky approach (Bauer et al., 2010; Geer and Bauer, 2011) where clear, cloudy and precipitating scenes are treated together, including scattering radiative transfer where necessary. This gives a wider observational coverage, and brings information on water vapour, cloud and precipitation into the analyses, benefitting forecasts (Geer et al., 2010; Cardinali and Prates, 2011). ECMWF are developing a cloud control variable, but even without one incremental 4D-Var is able to create and destroy hydrometeors in the model trajectory (Bauer et al., 2010). Hence it is worth seeing whether the all-sky approach can be applied to microwave sounders such as AMSU-A, and in particular, whether it can improve the assimilation of temperature information.

Table 1: Channel specifications of the AMSU-A instrument, ignoring purely stratospheric channels. Polarisation at nadir is either vertical (v) or horizontal (h) but varies across the scan.

Number	Frequency [GHz]	Polarisation (nadir)	NEΔT (specified) [K]	Peak of weighting function at nadir [km]	Surface to space transmittance at nadir [0-1]
1	23.8	v	0.3	0	N/A
2	31.4	v	0.3	0	0.94
3	50.3	v	0.4	0	0.67
4	52.8	v	0.25	1	0.31
5	53.596$\pm$0.115	h	0.25	4	0.12
6	54.4	h	0.25	7	0.02
7	54.94	v	0.25	10	0.00
8	55.5	h	0.25	14	0.00
15	89.0	v	0.5	0	N/A

Other NWP centres have attempted to account for cloud in AMSU-A radiances, for example by using cloud liquid water path as a bias predictor (Baker et al., 2005) or by directly assimilating radiances in all-sky conditions, in some cases using a cloud control variable (Ishibashi, 2011; Bauer et al., 2011). Documentation is as yet limited, but development is ongoing at JMA and NCEP / JCSDA. The Met Office assimilate cloud-affected AMSU-A radiances directly in their operational 4D-Var (English et al., 2007). They implemented a total water control variable, enabled cloud liquid water radiative transfer in the observation operator (though they did not simulate scattering) and added AMSU-A channels 1 and 2 to an existing system that was using channels 4, 5, 6 and various other stratospheric channels. Forecasts were clearly improved, but because the Met Office do not assimilate microwave imagers, the addition of AMSU-A channels 1 and 2 may well have been the most significant part of this upgrade, bringing completely new information on low-level moisture and cloud. Hence, the importance of all-sky radiative transfer for temperature sounding channels is not clearly proven by the Met Office work.

This work is laid out as follows: Sec. 2 looks at the information that AMSU-A can provide on cloud and temperature, Sec. 3 gives details of how the all-sky approach has been adapted to AMSU-A and Secs. 4 and 5 examine the results for channels 4 and 5. These results were not positive enough to justify introducing a costly and experimental new approach into the operational system, but developments will continue, and we will try to deal with some of the issues uncovered here.

2 Information content of AMSU-A

AMSU-A (Robel, 2009) is a 15 channel microwave radiometer for atmospheric temperature sounding that has been flown on NOAA polar orbiters starting with NOAA-15, as well as EUMETSAT's Metop-A. There are 12 channels in the 60 GHz oxygen band with weighting functions peaking from the surface to 40 km. There are also three imaging channels sensitive to water vapour, cloud and precipitation at 24, 31 and 89 GHz. Table 1 gives the specifications of channels relevant to the troposphere.

AMSU-A is a cross-track scanner, covering a swath of width 2343 km on the earth's surface. The swath is composed of thirty step-scanned observations with an effective field of view (EFOV) of 50 km by 50 km at nadir and 140 km by 80 km at the edge of the swath (Bennartz, 2000). The zenith angle varies from 1.5° to 58.5° over the same range. Clear-sky weighting functions for the tropospheric temperature channels are shown in Fig. 1. Channel 5 is the lowest channel operationally assimilated at ECMWF; so channels 3 and 4 could

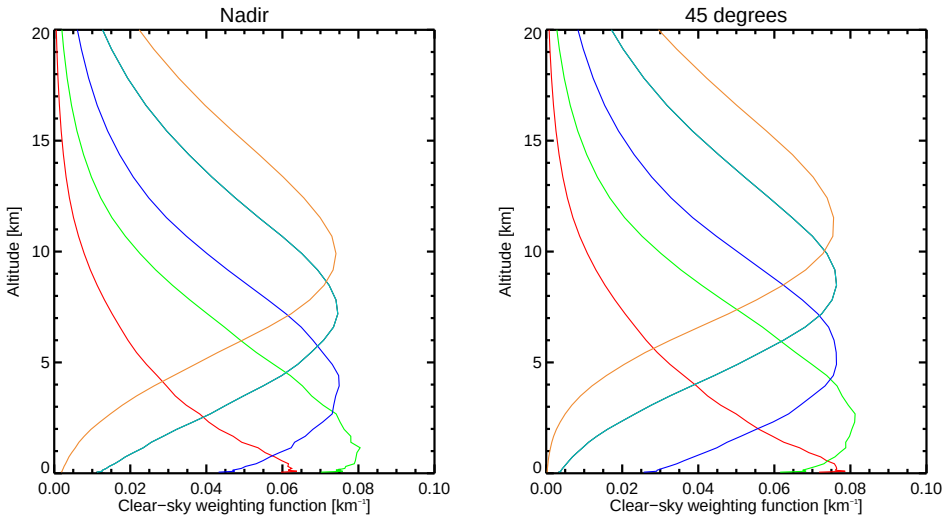

Figure 1: Global average clear-sky weighting functions at nadir (left) and at zenith angle of 45° (right) of AMSU-A channels 3 (red), 4 (green), 5 (dark blue), 6 (light blue) and 7 (orange). Weighting functions are computed as $-d\tau(lnP)/dlnP$ where τ is transmittance and P is pressure. The figure shows the global average of weighting functions computed from a large set of ECMWF atmospheric profiles.

bring new temperature information. Although we already assimilate channels with similar weighting functions from the infrared sounders AIRS and IASI (see appendix B for acronyms), microwave assimilation can bring greater coverage in cloudy areas, so there may be some new temperature information available.

Figure 2 shows the simulated radiative effect of hydrometeors on AMSU-A observations for 10th February 2011. This 'cloud effect' can be computed by assuming the all-sky brightness temperature T is the sum of a clear-sky part T_{clr} and a modification coming from cloud or precipitation, ΔT_{cld}:

$$T = T_{clr} + \Delta T_{cld} \tag{1}$$

Both clear-sky and all-sky brightness temperatures (T_{clr} and T) are routinely produced by the RTTOV-SCATT radiative transfer model (see e.g. Geer et al., 2009) so ΔT_{cld} can be computed easily. Areas of non-zero 'cloud' effect indicate the presence of radiatively important hydrometeors. For AMSU-A, the dominant effect is to increase brightness temperatures in the lower channels (e.g. 1 to 4) and to decrease them in higher channels (e.g. 5 and 6). Channels 1, 2 and 3 are window or near-window channels like those used in microwave imagers, where clouds and precipitation are warm emitters over a radiatively cold ocean surface. The dynamic range of the cloud signal is large, easily reaching 30 K. In contrast, channel 6 has a weighting function in the upper-troposphere and little sensitivity to the surface or even the lowest few kilometres of atmosphere. In this channel, hydrometeors reduce the brightness temperature in two ways: by moving the weighting function to higher levels where the temperature is colder, and through scattering, mainly from frozen particles. Channels 4 and 5 show a mix of behaviours: there are positive cloud effects from midlatitude cloud and precipitation, and negative ones from tropical deep convection. The effect of cloud is much smaller than in the window channels, with a dynamic range of a few Kelvin.

The Mie soft sphere approach used to compute snow scattering properties in RTTOV-SCATT is known to be unreliable (e.g. Petty and Huang, 2010; Kulie et al., 2010) and deep-convective regions are already screened out in the all-sky assimilation of microwave imagers due to an obvious problem of excess-scattering or excess falling snow coming from the model (Geer et al., 2010). To limit the effect of this problem in AMSU-A simulations, an ad-hoc 5 times reduction in model snow fluxes is used to decrease scattering at 50 to 60 GHz

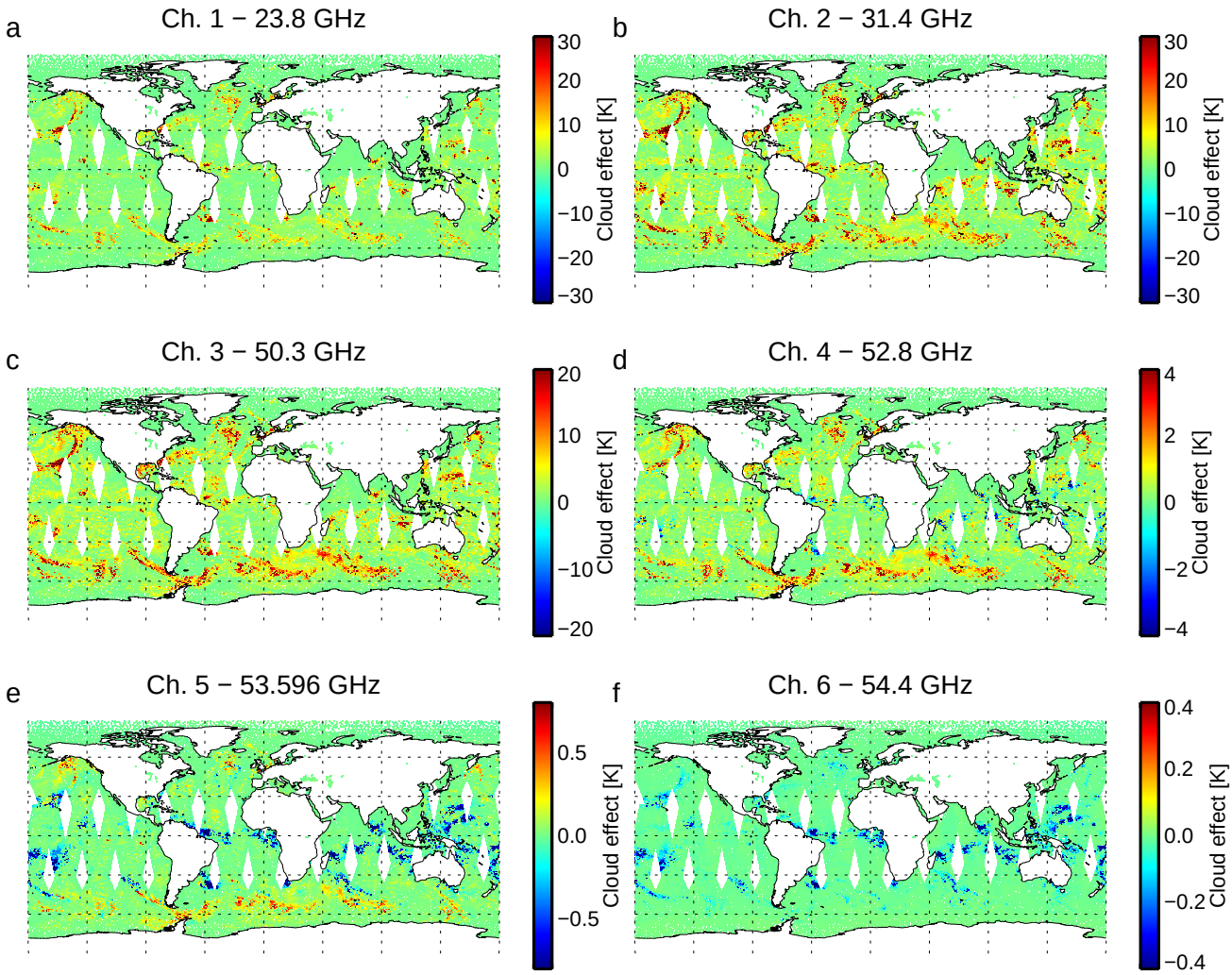

Figure 2: Effect of hydrometeors in K, computed as the difference between cloudy and clear first guess (FG) brightness temperatures. Sample is all Metop-A AMSU-A observations for 10th February 2011, but to reduce the size of the image file, they have been subsampled in longitude and latitude to one per 1° by 1° box. Sample is restricted to ocean and sea-ice surfaces.

and bring RTTOV-SCATT simulations closer to observations. Even if these problems were properly fixed, we would still not have any microphysical information on which to predict the habits of frozen precipitation or their size distributions, so it would be difficult to do accurate radiative transfer in such regions. Hence, there is no attempt to assimilate AMSU-A observations in tropical deep-convective regions. As done operationally for microwave imager channels with frequencies above 30 GHz, we will screen out these situations (see section 3.1).

We decided to focus our attention on a small subset of AMSU-A channels with the most potential benefit for temperature assimilation. Hence, channels 1 and 2 were ignored, being similar to those already assimilated from microwave imagers. Channel 3 would be difficult to use, because it has a blend of sounder and imager properties that vary across the swath. Early assimilation experiments with channel 3 showed an undesirable increase in the size of wind increments in the midlatitudes with corresponding degradations in the forecast scores, so to start with we ignored this channel too.

Channel 4, being sensitive to liquid water cloud as well as temperature and (to a small degree) water vapour, would be ideal for the all-sky approach, so it is our primary focus. However, early experiments with channel 4 showed a small but noticeable degradation of short-range forecasts in the midlatitudes, apparently coming from the 'cold-sector' bias that has affected the microwave imager channels for a long time (Geer et al., 2009; Geer and Bauer, 2010; Geer et al., 2011), and which is likely caused by a lack of liquid water cloud in the model boundary-layer stratocumulus associated with cold air outbreaks, which may be a general problem with cloud models (e.g. Klein et al., 2009). The bias was being aliased into the temperature and wind fields and hence causing forecast degradation. It is very difficult to correct the bias or even successfully identify all the affected areas. Hence we had to start by trying to assimilate channel 4 inside the range 40°N to 40°S, to avoid cold-sector biases.

Channel 5 shows a strong negative cloud effect from deep convection in the tropics, and we could not assimilate that data, but there is a positive signal in the midlatitudes coming principally from liquid water cloud. In the operational clear-sky assimilation, this signal could be aliased into temperature increments when cloud detection fails. Thus there might be benefits from taking proper account of the cloud signal by using the all-sky approach. Hence, channel 5 is the other main channel that we will look at. Channel 6 has an upper-tropospheric weighting function, so the precipitation and cloud it sees is predominantly frozen. Since we would have difficulty with the radiative transfer in such situations, we also ignored channel 6 to start with.

3 Method

3.1 Overview

Microwave imager radiances are assimilated operationally in all-sky conditions (Bauer et al., 2010; Geer et al., 2010; Geer and Bauer, 2011) using multiple-scattering radiative transfer from RTTOV-SCATT (Bauer et al., 2006). The all-sky approach has novel features to enable cloud and precipitation-affected assimilation:

- Observation errors are assigned as a function of 'symmetric' (or mean) cloud amount (Geer and Bauer, 2011);
- Observations are superobbed to give them a broader resolution (roughly 80 km by 80 km), one that is more representative of the model's effective resolution for cloud and precipitation (e.g. Geer and Bauer, 2010);
- Situations with large hydrometeor-related biases must be screened out. Examples are the 'excess scat-

tering' bias in deep convection, and the 'cold sector' bias in high latitude cold-air outbreaks discussed in the previous section.

The all-sky path omits some important aspects of the clear-sky framework, of which the most relevant are:

- The thinning algorithm selects observations with the smallest absolute first guess (FG) departures in channel 4, in order to reduce cloud-contamination.
- Each clear-sky observation has an associated skin-temperature sink variable to account for errors in the prescribed surface temperatures.

We decided not to incorporate either of these techniques in the all-sky framework. Actively thinning for cloud would clearly be inappropriate. As for a skin temperature sink variable, the operational microwave imager assimilation does not use one because (compared to land-surface temperatures) sea surface temperatures (SSTs) are well-specified, and the relatively low ocean surface emissivity also reduces the effect of any skin temperature errors.

In order to apply the all-sky approach to microwave sounders there were a number of issues. First, to specify the observation error we need to derive the mean cloud amount. For imagers, we rely on the normalised polarisation difference at 37 GHz as a measure of cloud amount (more precisely, of hydrometeor transmittance: Petty and Katsaros, 1990). Unfortunately, sounders such as AMSU-A measure only one polarisation, so we need another way to estimate cloud amount. Hence we make a liquid water path retrieval from the 24 and 31 GHz channels (Grody et al., 2001, and appendix A). Second, nadir scan positions see more cloud than the extreme positions, because (a) their weighting functions are lower in the atmosphere and (b) zenith and polarisation effects mean surface emissivity decreases slightly towards nadir, making the ocean surface relatively cooler and the clouds more visible. Hence, the observation error formulation will need to vary with scan position to account for the varying sensitivity to cloud. The effect of the differing resolutions of instrument and model also needs to be assessed, and in particular, the varying resolution across the AMSU-A swath. These issues are addressed in more detail in the following sections.

Due to the aforementioned problems modelling scattering from snow particles, we need to screen out the higher-frequency channels (above 30 GHz) in scattering situations. For microwave imagers, we use a threshold on mean cloud amount. For AMSU-A, we can use the 'cloud delta' (ΔT_{cld}, Eq. 1) instead. When this is negative, it is likely that scattering dominates the radiative transfer (though not guaranteed: absorption effects can also cause brightness temperature depressions). Screening is applied when either observed or simulated ΔT_{cld} is less than -0.5 K in channel 5, which typically removes 4% of observations.

3.2 Resolution and its variability with scan position

Conically scanning microwave imagers have a constant zenith angle, polarisation and field of view (FOV) size. Thus, instrument properties are constant from one observation to the next, which is very useful in all-sky assimilation, particularly because it makes it possible to create superobs at a given spatial resolution, simply by averaging all observations within the relevant grid box. This is important because the peak brightness temperature in any given area is generally associated with the heaviest precipitation. However, heavy precipitation is often localised, so where a small FOV can see a localised patch of very high brightness temperatures, a larger FOV will see an average of this and surrounding lower brightness temperatures. Hence the peak brightness temperature in any channel (and the precipitation response in general) is a function of FOV size, with larger FOVs seeing lower peak brightness temperatures. Hence it is important that the resolution of assimilated observations (or superobs) should roughly match the effective model resolution.

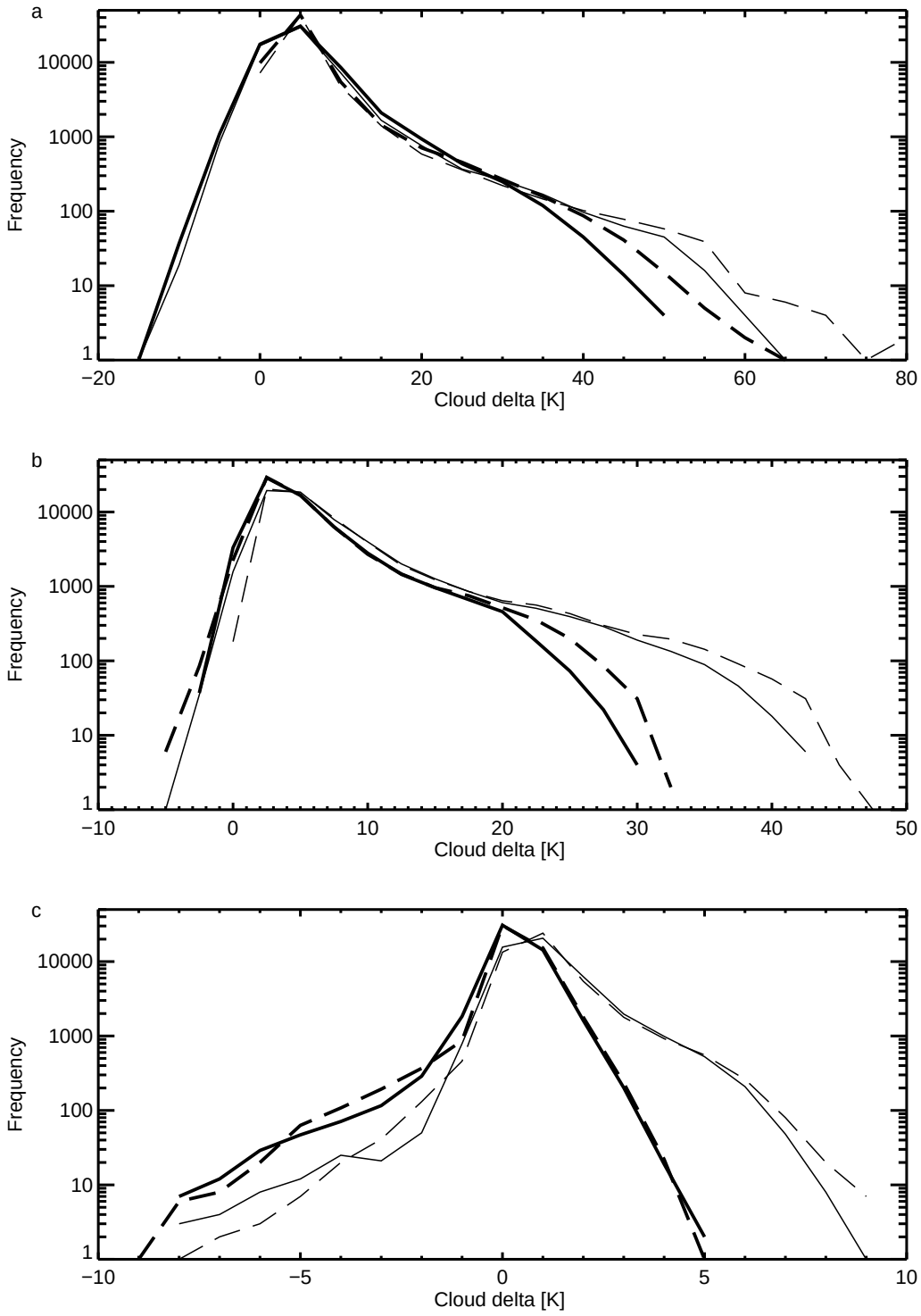

Figure 3: Histograms of cloud delta ΔT_{cld} in channels 1,3 and 4 (panels a,b and c) for extreme scan positions (4,5,26,27, thick line) and nadir scan positions (13-18, thin line) for observations (solid) and FG (dashed). Sample is the Metop-A observations of 5th February 2010, including scattering-affected situations.

By contrast, cross-track scanning radiometers have a varying zenith angle, polarisation and field of view. Thus, the radiative properties vary across the track. As mentioned, the EFOV of AMSU-A is 50 km by 50 km at nadir and 140 km by 80 km at the edge of the swath (Bennartz, 2000). In addition, Sec. 2 shows that at nadir AMSU-A sees deeper into the atmosphere and is more sensitive to cloud and precipitation compared to the higher zenith angles at the edge of the swath. Figure 3 examines the influence of these behaviours on the 'cloud delta' ΔT_{cld} (Eq. 1) in channels 1, 3 and 4. ΔT_{cld} is computed for both model and observations, using the modelled T_{clr} in place of the unknown 'observed' clear-sky TB, as this is quite accurate relative to errors in modelled cloud amounts (see Geer and Bauer, 2011). Positive cloud deltas are caused by relatively warm emission from cloud liquid and rain. In all three channels, the positive cloud delta is much greater for nadir scan positions than for extreme positions. In channel 4, for example, the cloud delta is a maximum of 5 K at extreme positions but 9 K at nadir, due to greater visibility of low clouds. This is true of both observed and modelled cloud delta.

In channel 1 there is no negative modelled cloud delta (dashed line) but there is apparently an observed effect (solid lines) as large as -10 K. In this channel there is no physical mechanism to produce a negative cloud delta, since both scattering and absorption from hydrometeors are too weak. Instead the apparent negative cloud deltas come from using the modelled T_{clr} in place of the unknown true value. Because forecast total column water vapour (TCWV) or modelled surface properties are sometimes incorrect, this can produce a T_{clr} that is on occasion higher than the observed all-sky brightness temperature T. By contrast, channel 4 is principally sensitive to temperature rather than TCWV or the surface, and temperature is very accurately forecast ($\simeq$0.2 K error). Hence the negative cloud delta is a real physical behaviour, coming from hydrometeor absorption at relatively cold upper levels, plus scattering. Interestingly, these effects are greater at high zenith angles, most likely coming from the increased optical path length.

In Fig. 3, the histograms of modelled and observed cloud deltas are quite similar, though modelled cloud delta peaks slightly higher (by $\simeq$10 K or 20% in channel 1 and by $\simeq$2 K or 7% in channel 3). This might be indicative of a model bias in highly precipitating situations, or a scale mismatch between observed EFOV and model effective resolution. However, it is clearly not a large effect, and it does not vary much between nadir and extreme scan positions. This shows that, to a first approximation, we can model the effect of cloud and precipitation on AMSU-A radiances without having to take into account changes in the EFOV size across the swath. Also, the EFOV appears roughly comparable to the effective resolution of cloud in the ECMWF system, so we do not need to make superobs either. However, to reduce data volumes and limit the effect of observation error correlation, we applied a thinning so that observations were limited to one per 80 km T255/N128 Gaussian grid box, with preference given to observations closest to the centre point of the box.

3.3 Prescribing the observation error

Observation error will be prescribed following the method of Geer and Bauer (2011). They modelled the variation of FG departures with cloud amount and used that model to predict the observation error. Simplifying slightly from their method, we ignore the contribution of background error to the FG departure standard deviations, and assume they directly represent observation error. For AMSU-A we also need to describe the variation of FG departures with with scan position, so we will add an extra term to the model. Hence, the observation error r will be prescribed as:

$$r = f(\theta)g(\overline{C_{LWP}}) \tag{2}$$

Here, $g(\overline{C_{LWP}})$ prescribes the observation error at nadir and is an increasing function of cloud amount, and $f(\theta)$ scales the error as a function of zenith angle θ. The mean cloud amount is computed as

$$\overline{C_{\mathrm{LWP}}} = (\mathrm{LWP_{OBS}} + \mathrm{LWP_{FG}})/2. \tag{3}$$

where LWP is retrieved from the brightness temperatures (see appendix, Eq. 11), with the retrieval applied separately to the observations and to the bias-corrected FG.

First we examined the variation of FG departures as a function of scan position, shown in Fig. 4. Near nadir (i.e. in the central scan positions) AMSU-A sounding channels see deeper into the atmosphere, giving a greater sensitivity to cloud and precipitation. Following Geer and Bauer (2011) that will naturally lead to larger standard deviations of FG departures. In practice, this effect is only seen in AMSU-A channels 3 and 4, and not in channel 1, 2 or 5. Hence it is presumably an effect of the visibility of the surface and of lower tropospheric cloud, rather than of deep convection. The same effect results in much larger FG departure standard deviations in channel 3 (order 3 K), compared to channel 4 (order 0.5 K) or channel 5 (order 0.25 K).

Trial and error showed that a Gaussian-like function can be used to model the variation in standard deviation with scan position:

$$f(\theta) = 0.3 + 0.7\exp\left(-\frac{(\beta\theta)^2}{2}\right) \tag{4}$$

Here, θ is the zenith angle in radians, and β=1.25 for channel 3 and 2.0 for channel 4. Figure 4 also shows the standard deviation of FG departures that have been divided by $f(\theta)$. Almost all variation with scan position has been eliminated. The scaling is relatively independent of cloud amount, whether for an all-sky sample (panel a) or just a 'clear-sky' sample (panel b, LWP $< 0.05\,\mathrm{kg\,m^{-2}}$ in both observation and FG). The scaling is optimised for the all-sky sample; it slightly over-corrects the extreme scan positions in clear-skies. English (2008) showed that even in clear-skies, forward modelling errors increase with visibility of the sea surface, due to errors in modelled skin temperature and emissivity. However, in all-sky assimilation, it is the visibility of cloud that is most important. For example, in channel 3, the cross-swath variation in error is about 1 K for the all-sky sample, but only 0.3 K for the 'clear' sample, and even that in reality contains some light-cloud situations. Nonetheless, Eq. 4 attempts to account for both surface and cloud effects.

The standard deviations of FG departures as a function of mean cloud ($\overline{C_{\mathrm{LWP}}}$, Eq. 3) are shown in Figure 5. Here, all FG departures have been rescaled by $f(\theta)$ to remove the scan-variation. Standard deviations vary as expected, i.e. values are low in clear skies, and then increase with cloud amount to a point where they start decreasing again (though not for channel 5). This decrease comes from the good agreement between observations and FG that is implicit when the mean cloud amount is high. The jagged lines for $C_{\mathrm{LWP}} > 1.0$ are due to inadequate sampling of the very small numbers of observations with large amounts of mean cloud.

Two samples are examined in Fig. 5, either with or without removing the 4% of points affected by scattering (which would not be assimilated in any case). The scattering points appear to be associated with the largest errors, particularly in channel 5. This would be expected given that in channel 5 scattering is the most important radiative effect of hydrometeors. Panel c is a clear confirmation of the need to remove scattering points, e.g. deep convective areas, before assimilating this channel. The dotted lines show a piecewise linear model for error:

$$\lambda = \left(\frac{g_{cld} - g_{clr}}{C_{cld} - C_{clr}}\right) \tag{5}$$

$$g(\overline{C_{LWP}}) = \begin{cases} g_{clr} & \text{if } \overline{C_{LWP}} \le C_{clr} \\ g_{clr} + \lambda(\overline{C_{LWP}} - C_{clr}) & \text{if } C_{clr} < \overline{C_{LWP}} < C_{cld} \\ g_{cld} & \text{if } \overline{C_{LWP}} \ge C_{cld} \end{cases} \tag{6}$$

Here, g_{clr} and g_{cld} are the minimum and maximum standard deviation of FG departures, as binned by mean cloud amount (e.g. 1.8 K and 12.5 K for channel 3), and C_{clr} and C_{cld} give the range of cloud amounts over which the main increase in error takes place (e.g. 0.01 to 0.47). These numbers were computed from an experiment with all-sky assimilation switched off inside a previous IFS cycle, simply by fitting by eye to figures like Fig. 5. These prescribed errors are slightly larger than the FG departure standard deviations in the active

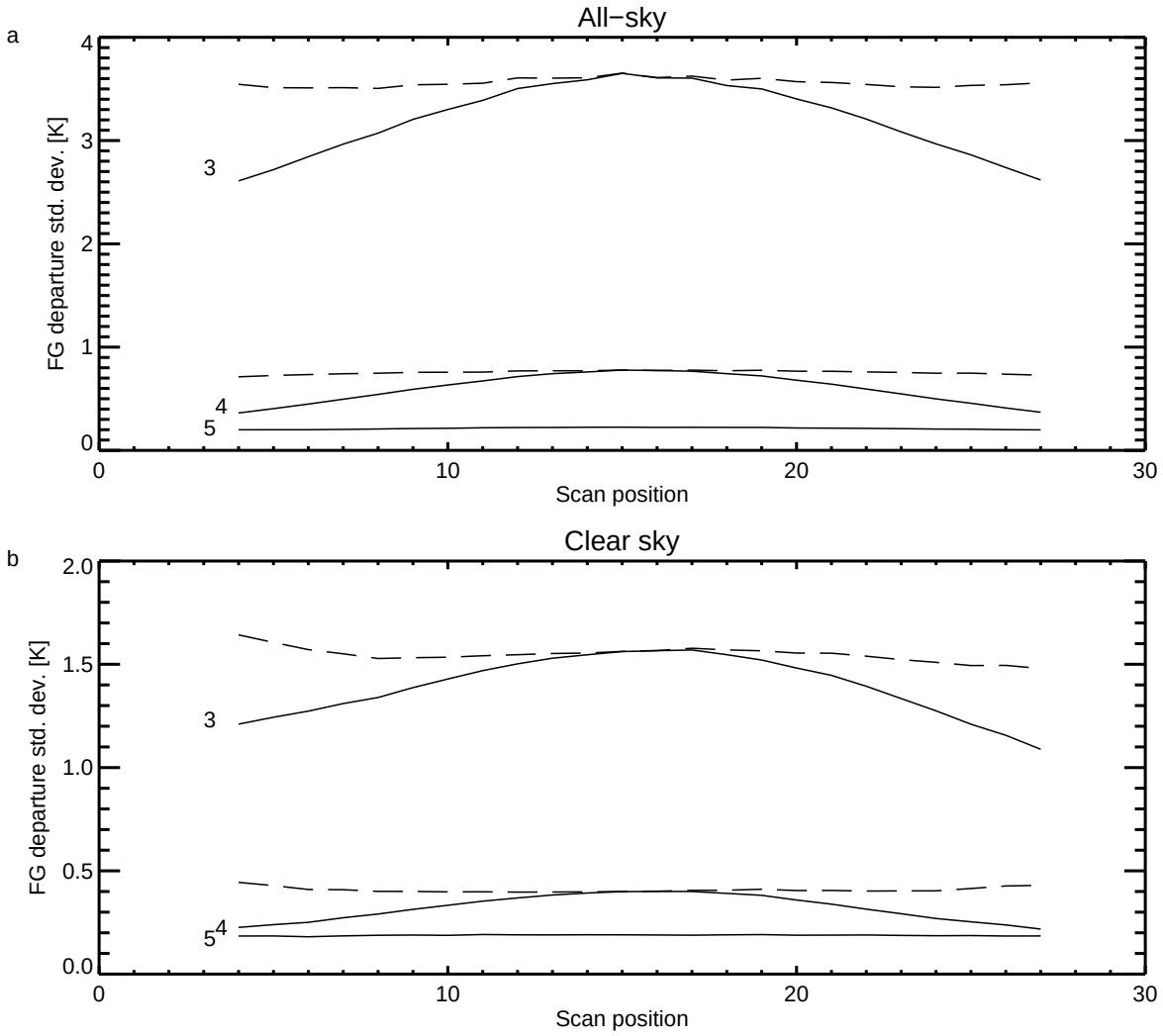

Figure 4: Standard deviation of AMSU-A FG departures in channels 3, 4 and 5 (solid lines, labelled on the figure) as a function of scan position. Also shown are the standard deviations of departures rescaled to remove the scan dependence in channels 3 and 4 (dashed lines, see text for details). Sample is 15 - 28 Feb 2011, 60°S to 60°N, ocean only for all-sky (panel a, $\simeq$ 3 million observations) or clear-sky (panel b, $\simeq$ 1 million observations with cloud liquid water path (LWP) $<$ 0.5 kg m^{-2} in both observation and FG). Scattering situations are excluded. Note that scan positions 1–3 and 28–30, which are truly the most extreme, are not used in the ECMWF system in the clear sky approach, and similarly they are ignored here.

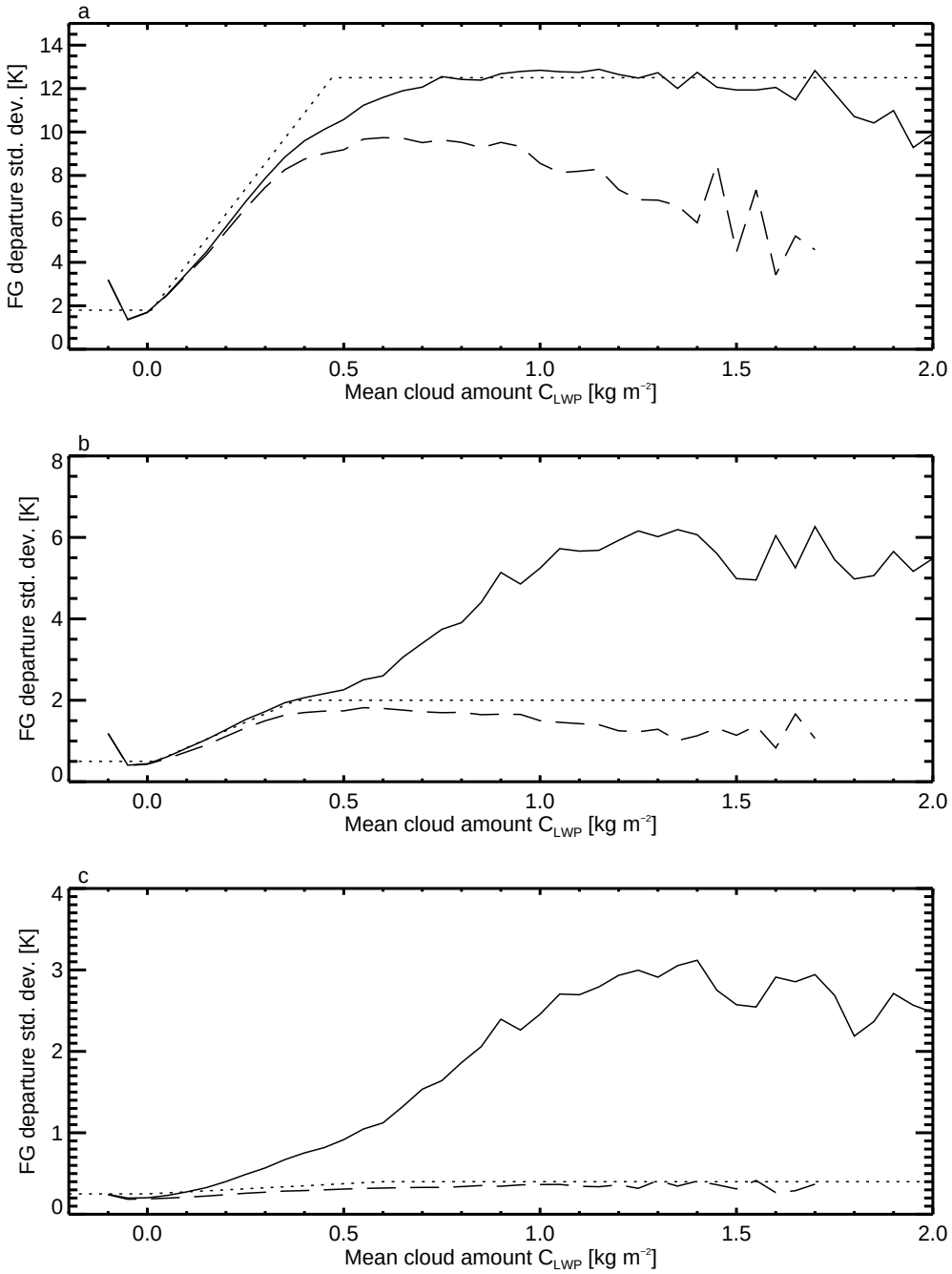

Figure 5: Standard deviation of AMSU-A FG departures in channels 3, 4 and 5 (panels a, b, and c respectively) as a function of mean cloud amount $\overline{C_{LWP}} = (LWP_{OBS} + LWP_{FG})/2$. FG departures have been re-scaled to eliminate scan-position dependence. Sample is as for Fig. 4 but either including (solid) or excluding (dashed) areas affected by scattering. Also shown is the model for FG departure standard deviation (dotted) which was fitted to an earlier cycle with larger errors, so it is now slightly over-cautious.

Table 2: Parameters for the observation error model, (Eqs. 2 to 6)

Channel	β	C_{clr} [kg m^{-2}]	C_{cld} [kg m^{-2}]	g_{clr} [K]	g_{cld} [K]
1	0.00	0.05	1.2	3.2	26.0
2	0.00	0.01	1.2	1.9	45.0
3	1.25	0.01	0.47	1.8	12.5
4	2.00	0.02	0.38	0.5	2.0
5	0.00	0.00	0.60	0.25	0.40
6	0.00	0.00	1.00	0.35	0.35

assimilation experiments at Cycle 37r2. However, in clear-sky assimilation we typically assign observation errors that are substantially larger than the FG departure standard deviation (e.g. Bormann et al., 2011b), so this may be no bad thing. Parameters for the error model are given in Tab. 2 for each of the channels we might assimilate.

Figure 6 tests the ability of the error model to describe AMSU-A FG departures. As shown in Geer and Bauer (2011), if the departures are normalised by the standard deviation of the whole sample, the distribution is far from Gaussian. In this erroneous constant-error approach, the normalised departures are too small in the majority of cases but too large in the cloudiest situations. This would lead to two problems: (a) cloud-affected observations would likely be rejected by quality control; (b) clear-sky observations would not have enough weight in the analysis. The new error model brings the distribution much closer to a Gaussian by assigning larger errors in cloudy situations and smaller ones in clear skies. The error model is fine for channels 3 and 4 but in channel 5 it gives errors that are always larger than the sample standard deviation (which is 0.21 K.) This is actually similar to what is done in the operational clear sky assimilation, where the observation error is set to 0.28 K for channel 5.

A test of the scan dependence of the error model is that the normalised FG departure standard deviation is constant and approximately equal to 1 in each scan position. This is true within $\pm$6% in all scan positions in channels 3 and 4, except positions 4 and 5 of channel 3, which go to +10% (figure not shown). Overall, it appears the error model works well for AMSU-A, simulating errors that increase with cloud amount and decrease towards higher zenith angles.

3.4 'Model-space' approach and performance

Recall that a 'model space' approach is used in the all-sky microwave imager assimilation (equivalently, mapping of model quantities to observation locations is done according to the nearest gridpoint, rather than by using bilinear interpolation from four surrounding points, as is conventional for most observation types). With this approach, the observation operator can be called just once per grid point, no matter how many observations are associated with that point. In the inner-loop minimisations, where the forecast model runs at a relatively coarse resolution, we have exploited this to provide a substantial computational cost saving in the operational microwave imager assimilation. This is not so easy to do for microwave sounders, because the zenith angle and polarisation vary. When several AMSU-A observations have a similar zenith angle (to within 0.2°) and are associated with the same gridpoint, we can still economise and use a single radiative transfer simulation. The performance saving is beneficial but not as great as for the imagers. Hence it is more computationally demanding to assimilate a cross-track sounder than a conically-scanning imager (given the same number of channels), and all-sky is very much more demanding than the clear-sky approach. This is a disadvantage for the new technique and it means that we must be economical with the number of channels to which it is applied.

A second issue is that the 'nearest gridpoint' temperature profile is not appropriate for temperature-sounding

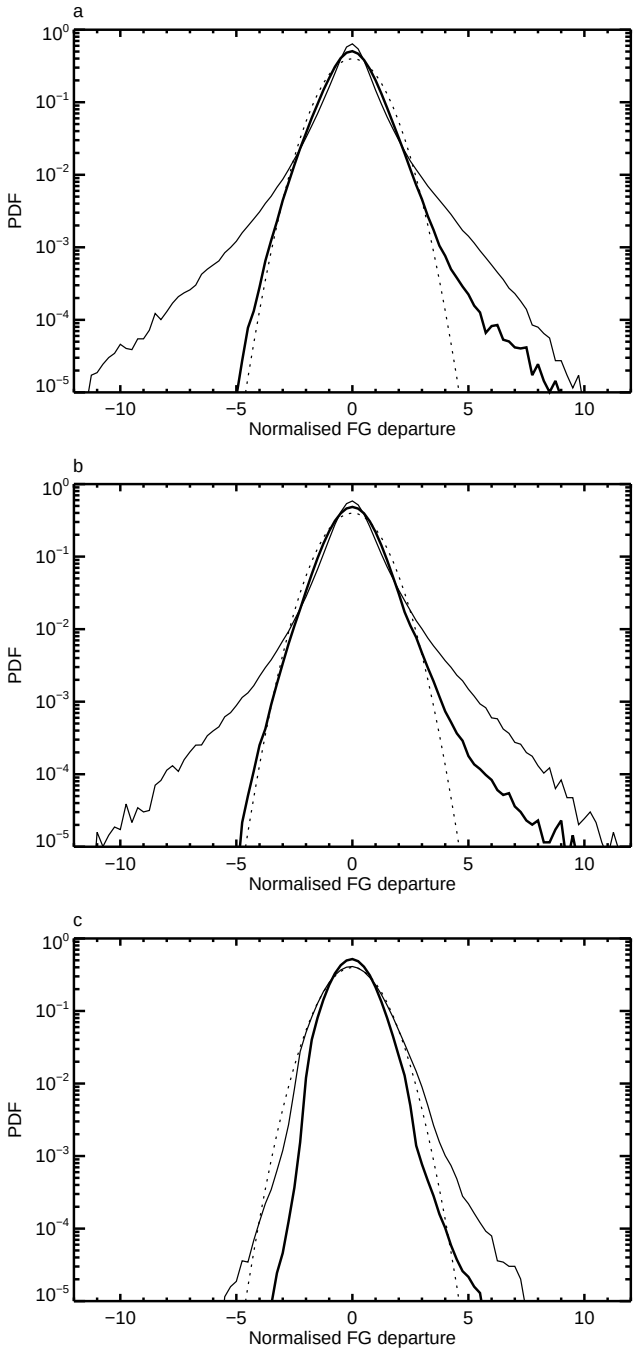

Figure 6: Histograms of FG departures in channels 3, 4 and 5 (panels a, b, and c respectively) normalised by the sample standard deviation (thin solid) or by the error model (thick solid). Sample excludes areas affected by scattering. Also shown is the Gaussian function (dotted). Vertical axis is logarithmic to emphasise the wings of the distribution.

Experiment			
Name	Control	Clear-sky	All-sky
ID	fim0	fimy	fivd
Treatment of AMSU-A ch. 4			
Assimilated	No	60°N to 60°S	40°N to 40°S
Radiative transfer	-	Hydrometeors ignored	Hydrometeors included
Observation error	-	0.3 K	Variable (Geer and Bauer, 2011)
Cloud screening	-	Yes	No

Table 3: Channel 4 experiment configuration.

channels in regions of strong horizontal temperature gradients, such as around the polar front. To demonstrate this, brightness temperatures were simulated using a FG temperature profile coming either from the nearest grid-point or from an interpolation to the observation location. In the region of the polar front, the difference between the two approaches had a standard deviation of 0.07 K in brightness temperature and a Moiré pattern associated with the interaction between the observation scan pattern and the model grid (not shown). While this error is substantially smaller than the specified instrument noise (Tab. 1) it is still worth taking seriously. Hence a hybrid approach is used for AMSU-A: the model temperature profile is interpolated to the observation location while the pressure and hydrometeor profiles remain those of the nearest gridpoint.

4 Results for channel 4

4.1 All-sky and clear-sky use of channel 4

4.1.1 Experiment design

This section compares the clear-sky and all-sky approaches for assimilating channel 4. The experiments are summarised in Tab. 3. Channel 4 assimilation is done over ocean surfaces only and not over land or sea-ice. Exactly the same set of channel 4 observations are used in each experiment, aside from the differences listed in the table. To achieve this, the clear-sky channel 4 assimilation was carried out in the all-sky framework but with cloud and precipitation radiative transfer turned off. This ensured we used the same thinning pattern and screening criteria in both experiments and avoided other complications such as whether or not to use a skin temperature sink variable. In the clear-sky approach, cloudy scenes are eliminated using a threshold of $0.02\,\mathrm{kg\,m^{-2}}$ in observed LWP (retrieved via Eq. 11), and a flat 0.3 K observation error is prescribed (justified from FG departures). The all-sky approach is restricted to the range 40°N to 40°S because of cold-sector cloud biases. Note that there has been no attempt to find the very best clear-sky implementation: perhaps improvements could come from the use of scan-dependent observation errors, or an even tighter cloud-screening. This 'clear-sky' experiment gives a first-order estimate of how clear-sky channel 4 assimilation would behave.

Experiments are based on cycle 37r2 of the ECMWF operational NWP system, but with a slightly reduced horizontal resolution of T799 (roughly 25 km). These experiments run the delayed-cutoff 12 h analysis but not the 6 h early-delivery analyses (see Haseler, 2004). Variational Bias Correction (VarBC Dee, 2004) has been spun-up in advance, so there is no need to eliminate any further spinup period. The control provides initial conditions for the other experiments, which start on 7 February 2011 and run to 30 April.

The full operational observing system is used including polar orbiting satellite measurements (AMSR-E, SSMIS, HIRS, AMSU-A, AMSU-B, MHS, AIRS, IASI TBs, QuikSCAT wind - see appendix B for acronyms not

yet defined), geostationary radiances and wind vectors (SATOB-uv), radiosonde temperature, specific humidity and wind measurements (TEMP-T, TEMP-q and TEMP-uv), surface pressure data (SYNOP-Ps) and aircraft temperature reports (AIREP-T). When passing AMSU-A data through the all-sky system, we use observations from NOAA-15, NOAA-18, NOAA-19 and Metop-A but not Aqua because channels 4 and 5 have become too noisy in recent years and have not been used operationally in clear skies since April 2010.

4.1.2 Scores and observation fits

Figure 7 shows the effect on RMS forecast scores for vector wind over an 83-day experimental period. The y-axis is restricted to no more than $\pm 3\%$, so we are looking at extremely small changes in the scores. Clear-sky channel 4 assimilation has no significant impact at all, whereas all-sky assimilation makes both negative and positive impacts. Ignoring the scores at T+12, which simply show the change in the RMS increment (Geer and Bauer, 2010), all-sky channel 4 makes significant degradations of 0.6% to 0.7% at days 2 to 4 in the NH in the lower troposphere at 850 hPa, counterbalanced by improvements in tropical scores at day 4 at 500 hPa (0.8%) and days 2 and 3 at 850 hPa (0.5% to 0.7%). There are some other improvements, particularly around day 3 in the SH, but these are not significant. In geopotential scores in the extratropics there is a roughly similar picture (not shown). Relative humidity and temperature scores degrade in the early forecast period (not shown) but these are particularly responsive to increased activity in the increments. Overall, the forecast scores for the all-sky assimilation are quite promising.

The quality of temperatures in the analysis and early forecast range can be examined using observation fits. For IASI in the tropics (top panel, Fig. 8), both clear-sky and all-sky approaches improve fits in the window channels (about 500 to 700) and in the WV channels (the last 10, i.e. 2889 to 5480), though these improvements are extremely small (of order 0.1 - 0.4%). The extratropics show minor degradations of around 0.2 - 0.3% at FG (bottom panel, Fig. 8) for both all-sky and clear-sky. In the NH in particular, all-sky slightly worsens the IASI analysis fit and reduces the number of IASI lower-tropospheric observations by around 0.5 - 1% (not shown). This may be consistent with the slightly degraded NH forecast scores in Fig. 7. A broadly similar picture is seen in in-situ AIREP temperatures, where FG fits are slightly improved (order 0.4%) in the tropics but they are unaffected in the NH (not shown). In contrast, there are no degradations in fits to clear-sky AMSU-A channels, though the improvements are concentrated in the tropics (Fig. 9). Standard deviations of analysis departures from AMSU-A channel 5 are slightly reduced by the assimilation of channel 4 in either the all-sky or the clear-sky route. The all-sky approach shows the best improvement in the FG, of about 0.3 - 0.4% in channels 5 and 6.

Fits to the microwave imagers show a more uniformly positive impact from all-sky assimilation; the imagers have relatively little sensitivity to temperature and instead they primarily sense the moist variables. Fits to AMSR-E in Fig. 10 are improved by around 0.5% to 3% in the analysis and 0.5% to 1.5% in the FG, indicating improved hydrometeor or water vapour fields. These improvements are present in both the tropics and extratropics, and are largest in the tropics (not shown). HIRS channels 7, 11 and 12 and AMSU-B channels 3 to 5 (not shown) are assimilated in clear-skies and are partly or completely water vapour channels. These channels are improved in the tropics by about 0.5% in both analysis and FG in both clear-sky and all-sky experiments. However, the improvement in AMSR-E fits is much bigger with all-sky, particularly in channel 10 (37h) which is the most sensitive to cloud water. This suggests that both clear-sky and all-sky channel 4 make a slight improvement to the tropical humidity distribution (of up to 0.5% in observation space) but only the all-sky approach can make an improvement in cloud water (order 3%).

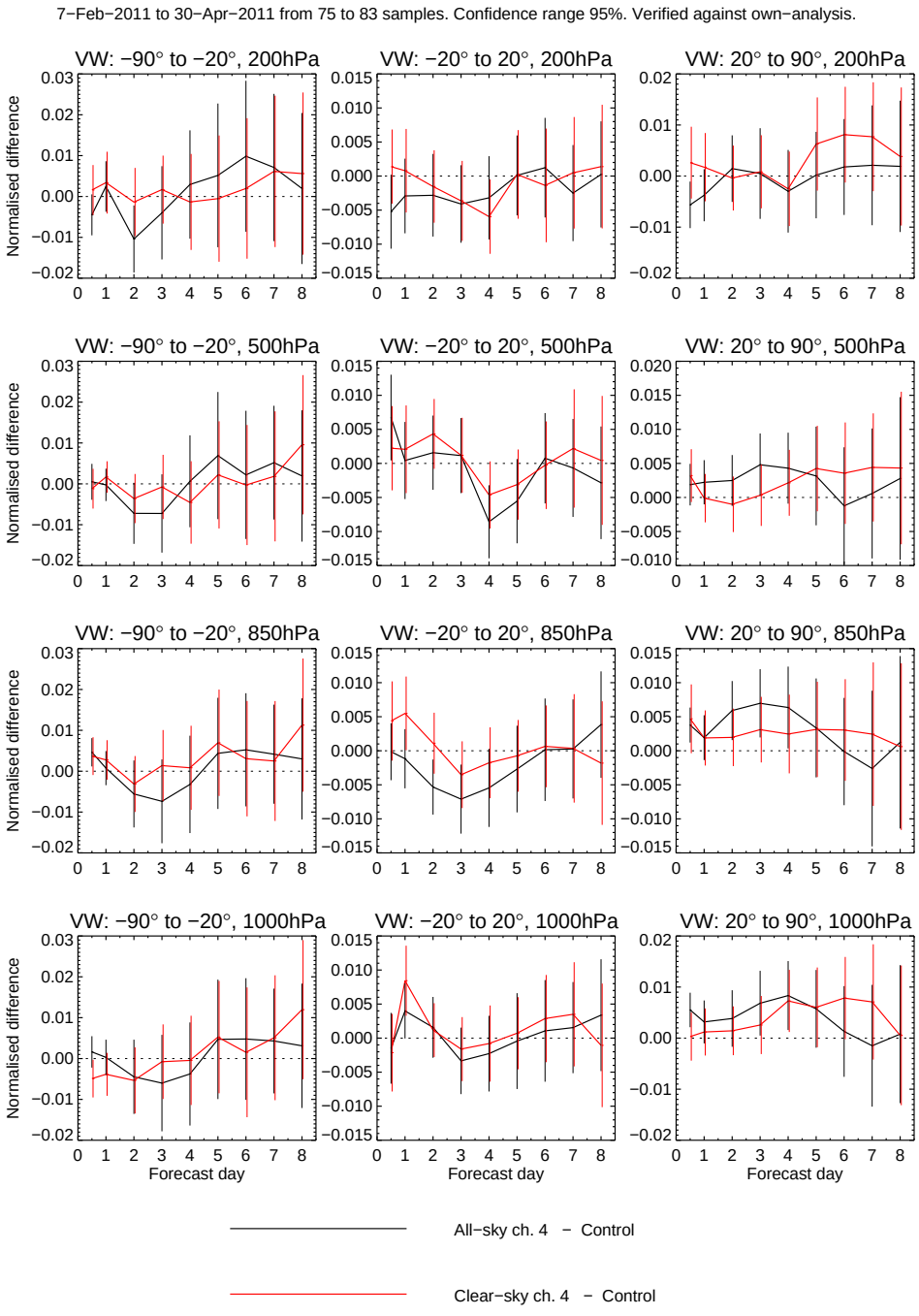

Figure 7: Effect of assimilating all-sky AMSU-A channel 4 radiances. Normalised difference in RMS vector wind forecast error between experiment and control, using own-analyses as the reference.

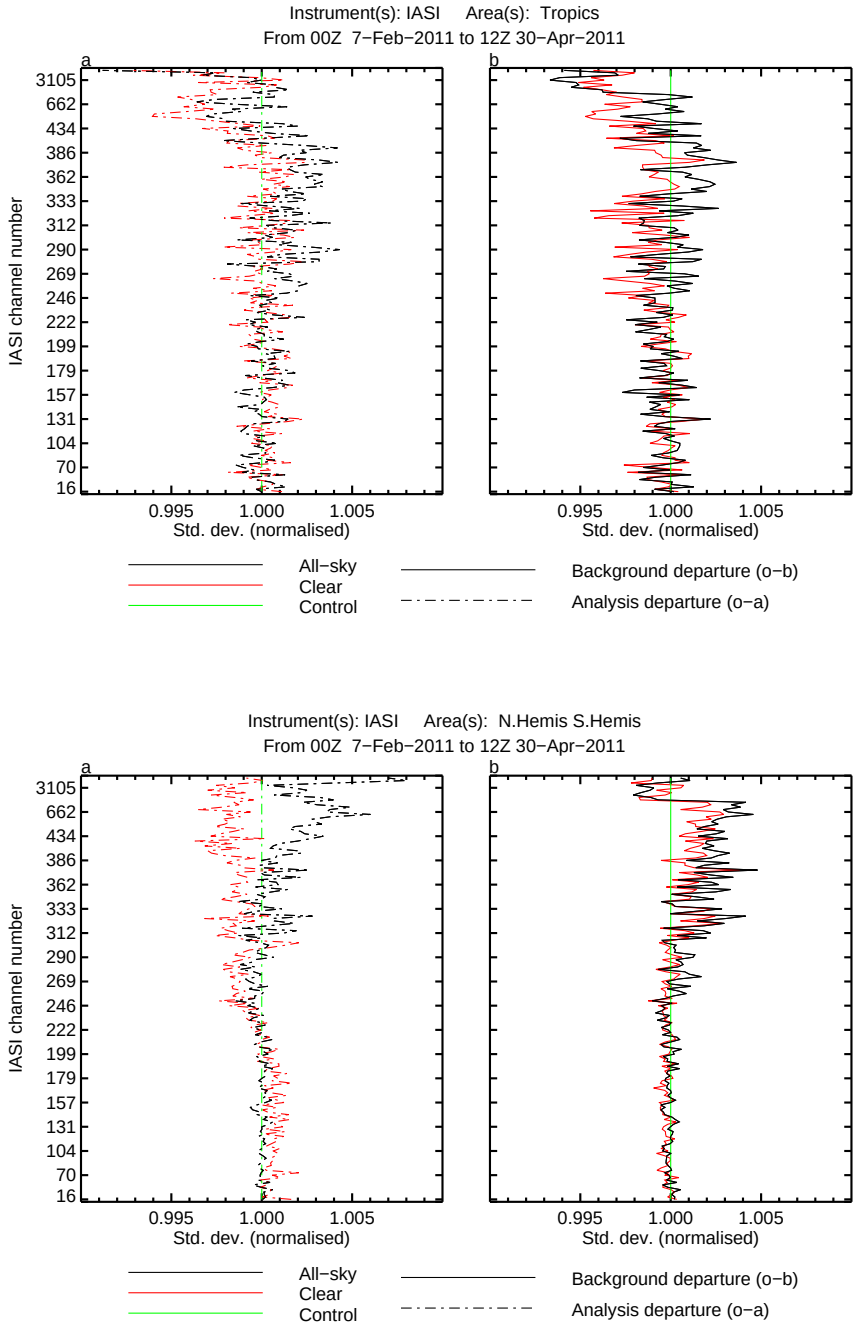

Figure 8: Standard deviation of (a) analysis and (b) FG departures from assimilated IASI radiance observations in the tropics (top) and extratropics (bottom). Standard deviations have been normalised by the control values. Only assimilated channels are shown; there are ten channels per division on the y-axis. IASI channel number n can be related to wavenumber $\overline{\nu}$ by the formula $n = 4(\overline{\nu} + 645cm^{-1})$

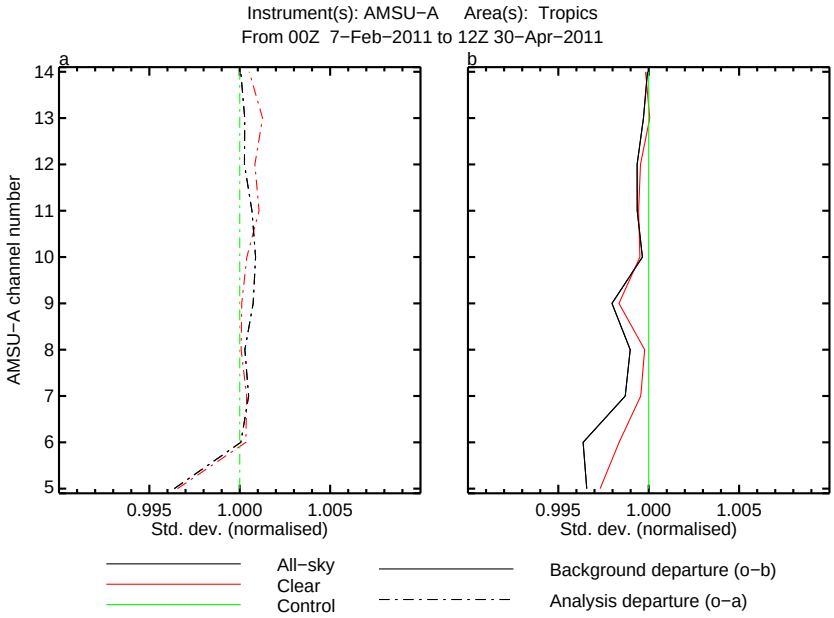

Figure 9: As Fig. 9 but for AMSU-A clear-sky channels

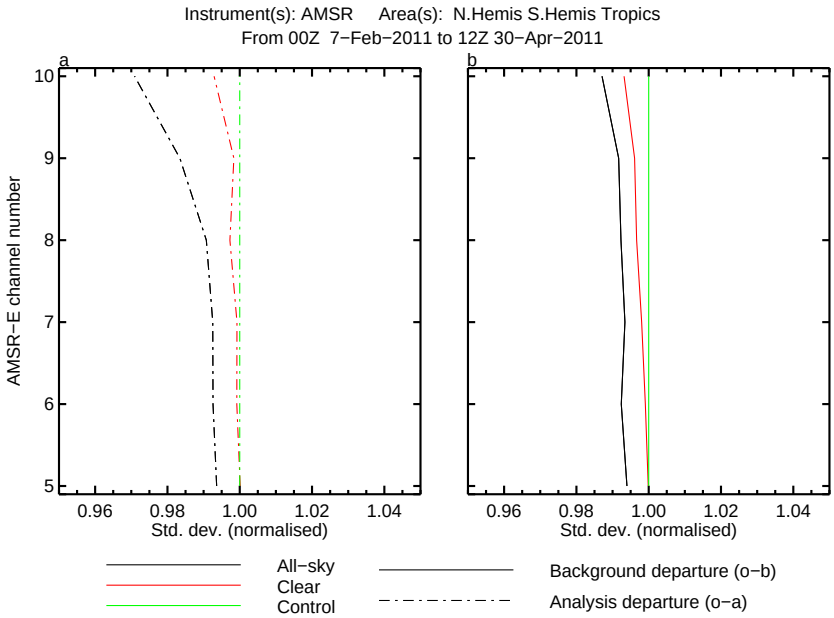

Figure 10: As Fig. 9 but for AMSR-E.

4.1.3 Analyses and increments

The difference between the all-sky and clear-sky assimilation of channel 4 is particularly evident in the analysis increments. Figures 11 and 12 show the mean change in analysed temperature at 850 hPa and 925 hPa, as well as the mean increments in the control experiment. These mean increments are intended to give some feeling for the significance of the temperature changes. At 850 hPa, all-sky channel 4 assimilation increases analysed temperatures by up to 0.3 K in some regions of trade cumulus close to the ITCZ. The clear-sky experiment does not show this, so the effect probably comes through the cloud physics in the all-sky approach. It is likely that biases between modelled and observed cloud fields are being aliased into the temperature field at the top of the tropical boundary layer. The clear-sky approach is not perfect either, and there are increases of up to 0.6 K in marine stratocumulus regions at 925 hPa which probably come from undetected cloud being aliased into the temperature field. However, in the context of the larger battle between model and observations that is represented by the mean increment field, these biases in channel 4, whether in clear-sky or all-sky, are relatively modest.

Using a number of single-cycle experiments with a common FG, by switching different channels on or off, it is possible to compute the part of the increment field coming from any particular channel or instrument. Figure 13 shows the global RMS of increments computed using these methods. Concentrating on the curves for all-sky or clear-sky channel 4, it is seen that all-sky increments are always larger, and there is a particular large bulge at 850 hPa in temperature (and to a lesser degree in specific humidity and cloud liquid water). Also shown are the increments from the assimilation of the three all-sky microwave imagers (TMI, SSMIS F17 and AMSR-E) and these are quite similar in shape to the all-sky AMSU-A channel 4 increments, although larger in magnitude. By contrast, the shape of the clear-sky channel 4 increments is much closer to those from AMSU-A channel 5, which is assimilated through the clear-sky approach. This suggests that all-sky and clear-sky increments largely come through different mechanisms. For example, all-sky temperature increments could come either directly through sensitivity to temperature, via the tracer effect of 4D-Var and the sensitivity to humidity (though this effect is likely small), or through the adjoint of the model physics and the sensitivity to cloud. Clear-sky increments would mostly come through the direct sensitivity to temperature.

To further illustrate the difference between the clear-sky and all-sky approaches, Fig. 14 shows the temperature increments caused by AMSU-A channel 4 on model level 83 (about 954 hPa) at the beginning of the assimilation window, as derived from the single-cycle denial experiments. By eye (and indeed by more quantitative methods) there is very little correlation between the patterns of increments in the all-sky and clear-sky approaches. This supports the conclusion that even when applied to the same channel, all-sky and clear-sky assimilation make temperature increments through different mechanisms, with the sensitivity to cloud being dominant in the all-sky approach.

4.1.4 Summary

Clear-sky channel 4 assimilation brings useful information on temperature and water vapour, as evidenced by improved fits of up to 0.5% to HIRS, AMSU-A, AMSU-B and AMSR-E at analysis and FG (e.g. Figs. 9, 10) and IASI at analysis (Fig. 8). However, these improvements do not translate into forecast score improvements, and perhaps this is explained by the fact that the infrared sounders AIRS, IASI and HIRS are already strongly constraining lower tropospheric temperatures through their window channels and lowest-sounding CO_2 channels. Indeed, there may be some conflict between AMSU-A channel 4 and IASI, as shown by the order 0.2% degradation in extratropical fits at FG (Fig. 8). Also, as shown by Fig. 1, the AMSU-A channel 5 and channel 4 weighting functions have a substantial overlap, so channel 4 does not bring completely new information.

In contrast, the assimilation of AMSU-A through the all-sky route has its biggest impact on cloud water, as

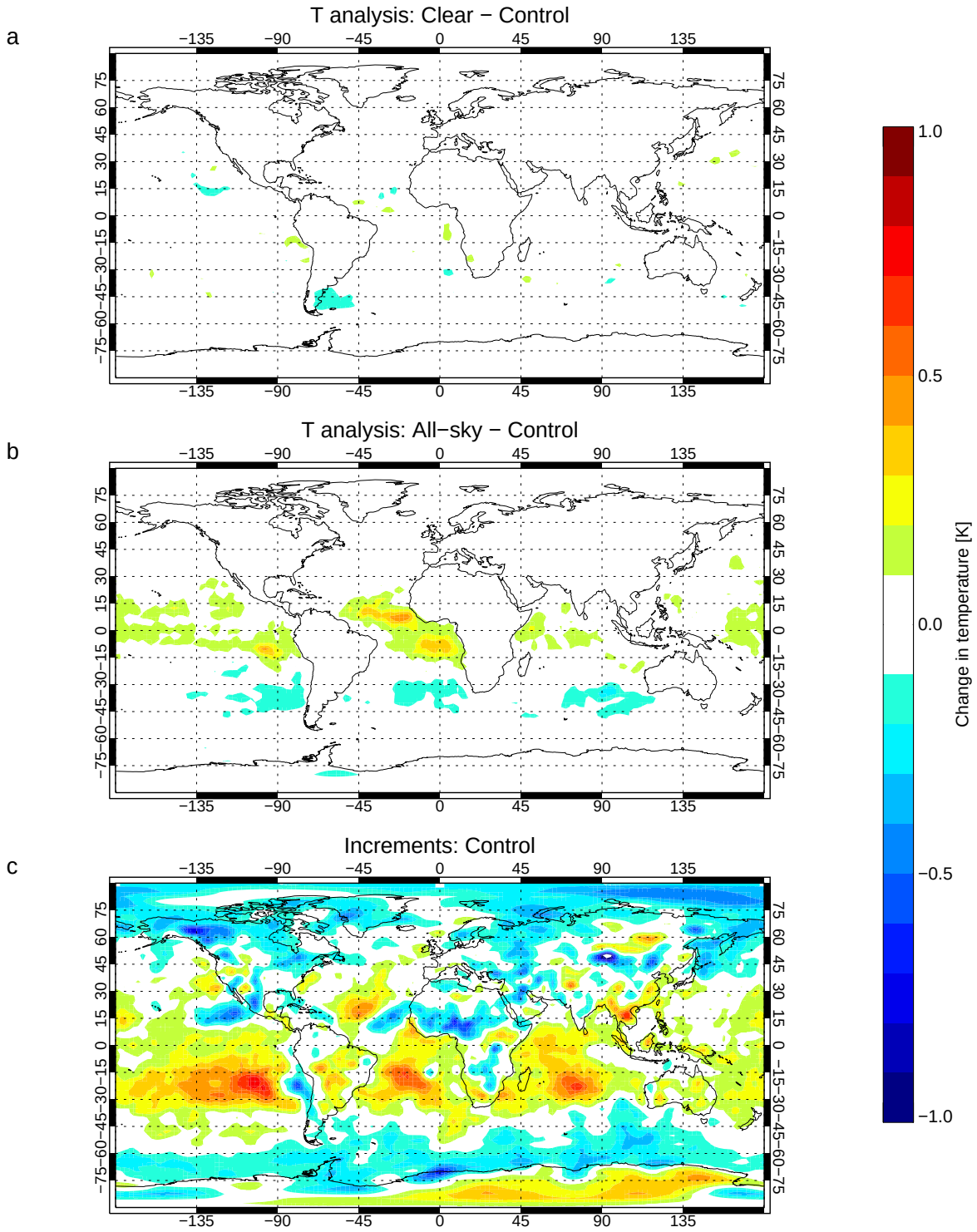

Figure 11: Temperature fields at 850 hPa: (a) Mean difference between Clear and Control analyses; (b) Mean difference between All-sky and Control analyses; (c) Mean temperature increments in the Control. Statistics are computed over the period 7 Feb - 30 Apr 2011, based on 00Z and 12Z analyses (panels a and b) and 12Z analysis minus FG (panel c).

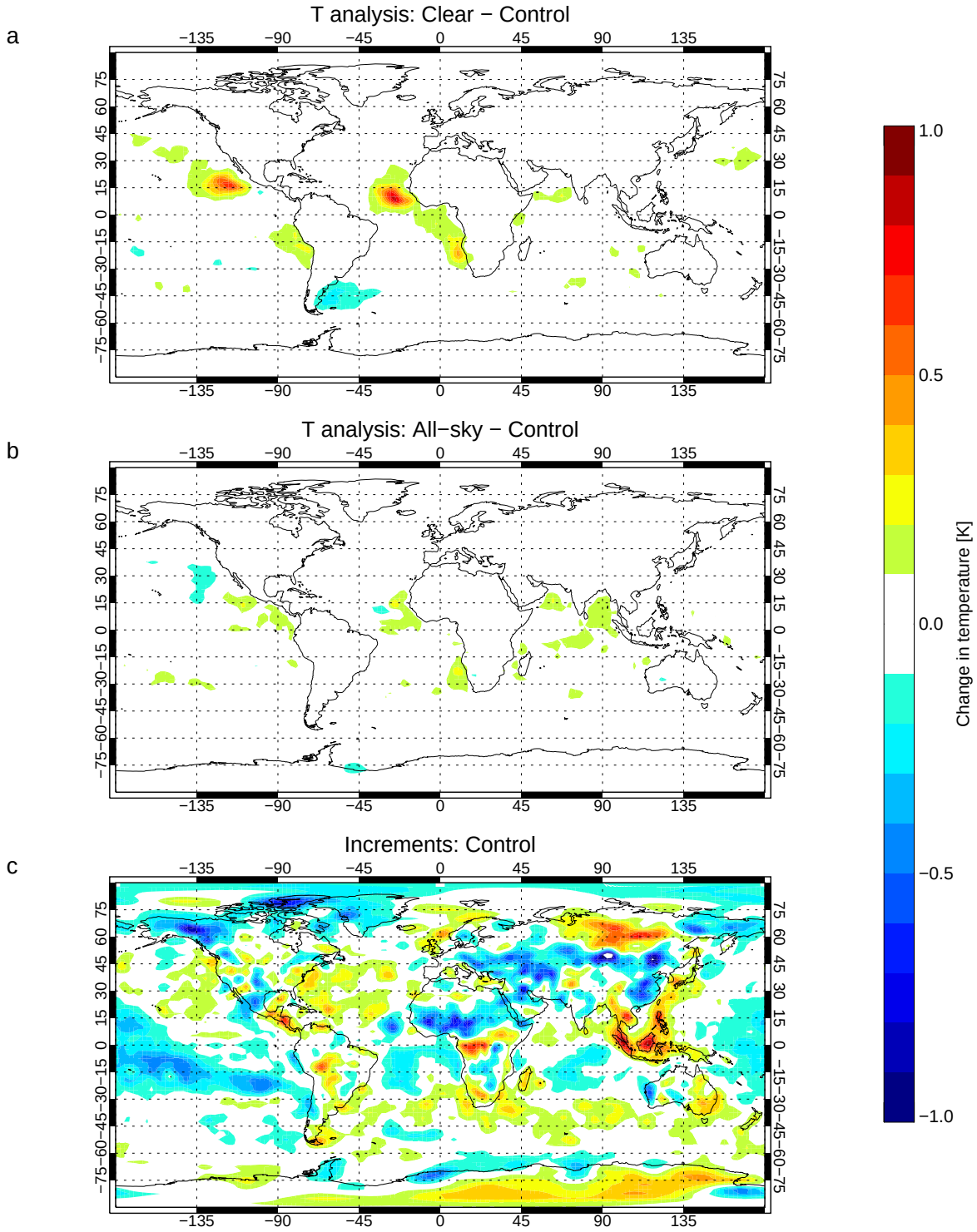

Figure 12: As Fig. 11 but at 925hPa.

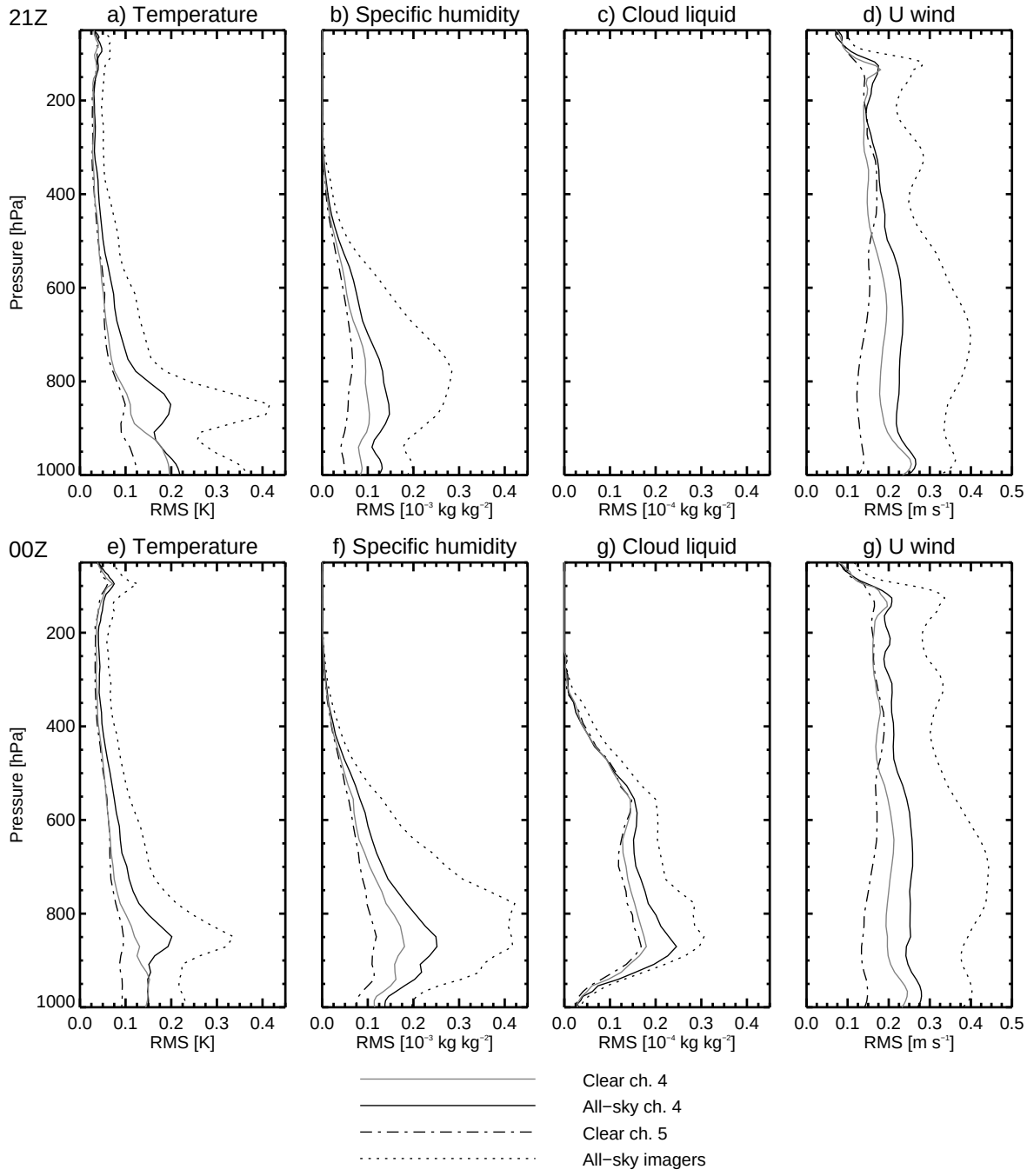

Figure 13: RMS of increments between 40°S and 40°N at the beginning of the assimilation window (a-d) or three hours in (e-h) coming from either clear-sky ch. 4 AMSU-A (grey solid), all-sky ch. 4 AMSU-A (black solid), clear-sky ch.5 (dot-dash) or all-sky microwave imagers (dotted) based on single-cycle experiments with a common FG at 21Z on 14 Feb 2011. There is no cloud liquid water (CLW) control variable as yet, so the 00Z CLW increments are zero.

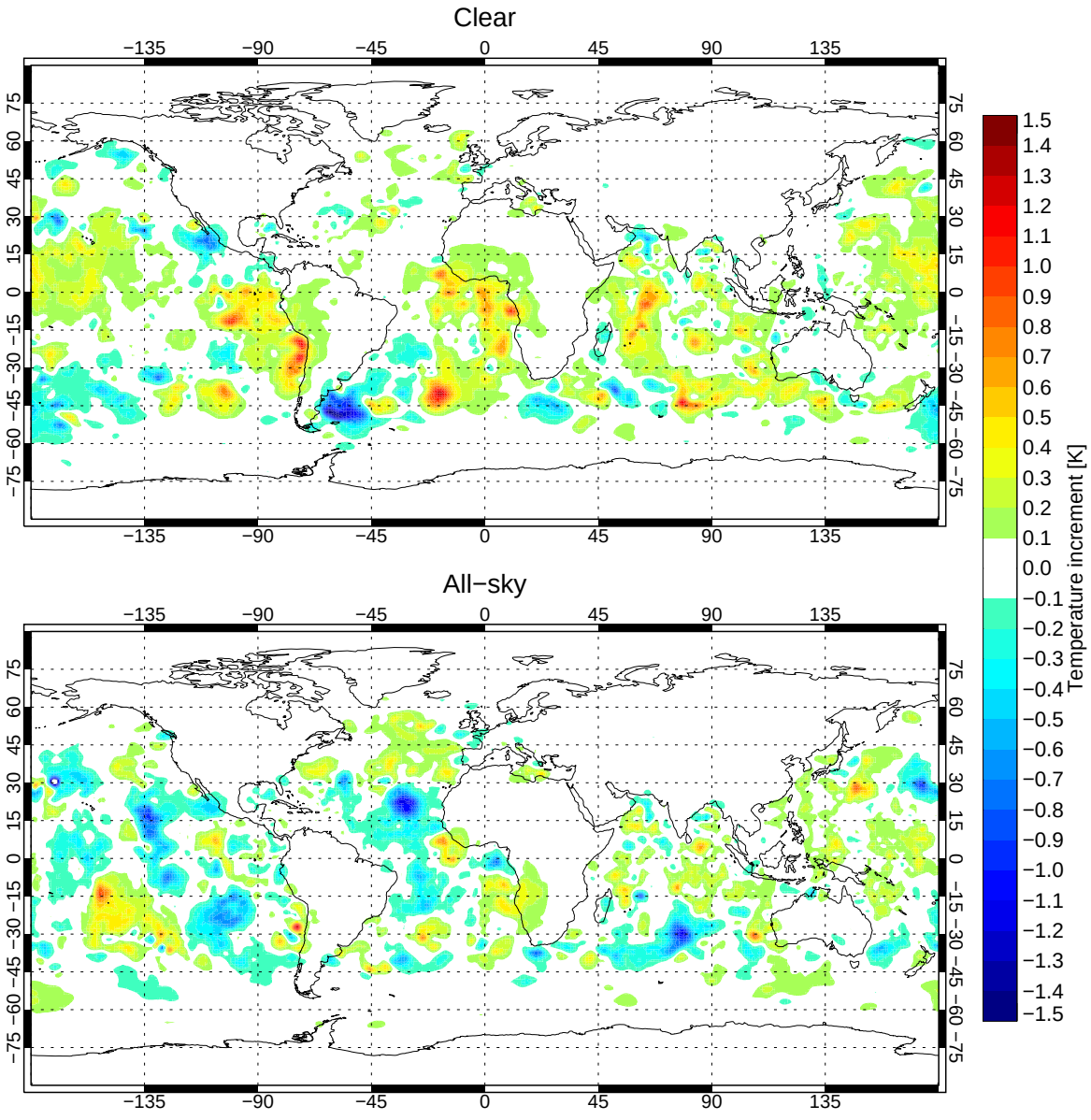

Figure 14: Temperature increments at the beginning of the window on model level 83 (about 954 hPa) coming from the assimilation of (a) clear-sky channel 4; (b) all-sky ch. 4. Date is 21Z on 14 Feb 2011.

Experiment name	ID	Dates
Winter AMSU-A	fl7f	17 Jan – 28 Feb 2011
Winter control	fkvl	
Summer AMSU-A	flcm	11 Jun – 14 Jul 2011
Summer control	fkvq	

Table 4: Configuration of the cycle 37r3 experiments.

shown by a 3% improvement in analysis fit to AMSR-E channel 10 (37h, Fig. 10). This goes with an improvement in forecast scores of up to 0.7% at days 2-4 in the tropics, though there are also degradations in NH scores (Fig. 7). However, there is an increase in RMS analysis increment 'noise' at 850hPa (Fig. 13).

4.2 Tests at 37r3

4.2.1 Experiments and forecast verification

With the promising results of the tests at 37r2, it was hoped that all-sky channel 4 assimilation could be included in a future operational cycle. Experiments were performed at cycle 37r3 with a view to including channel 4 operationally in 38r1 (Tab. 4). A resolution of T511 was used. As for the experiments at 37r2, we used four AMSU-As: those on NOAA-15, NOAA-18, NOAA-19 and Metop-A. The effect of all-sky AMSU-A channel 4 on fits to other observations was similar to the 37r2 experiments. As before, the most obvious improvement came in AMSR-E observations sensitive to liquid water cloud (not shown). However, the forecast scores came under greater scrutiny and ultimately, all-sky AMSU-A channel 4 was not considered suitable for operational use.

For forecast scores, the summer and winter runs have been combined to give about 10 weeks of verification. The normalised changes in RMS errors in wind and temperature are shown in Figs. 15 and 16 as a function of latitude and pressure. The change in wind errors is almost always insignificant, though there is a slight increase in the RMS errors in the first 24 h. As mentioned before, an increase in RMS errors at T+12 in own-analysis scores is equivalent to an increase in the size of the analysis increments. Temperature errors in the tropics at around 850 hPa show a significant degradation. At T+12, this is again just a reflection of larger temperature increments, but there are also degradations that persist to the end of the forecast range. These are explained by a 0.05 K increase in the tropical mean analysed temperature at 850 hPa, similar to what was seen in the 37r2 experiments in Fig. 11. It was this apparent increase in temperature RMS errors at 850 hPa that was the main concern for operational use.

4.2.2 AMSU-A channel 4 in a wider context

The increase in temperature RMS errors at 850 hPa is a well-known feature of the all-sky system. In fact, the addition of microwave imagers causes much greater mean changes in the temperature and water vapour field (and consequently larger changes in RMS forecast scores) than does the addition of AMSU-A channel 4. Figures 17 and 18 show the mean tropical (20°N to 20°S) temperature and relative humidity as a function of forecast hour. Four short experiments have been performed, starting from a baseline of the full operational observing system but with microwave imagers removed. The 'control' adds all-sky imagers TMI and SSMIS F17, giving the operational configuration following the loss of AMSR-E in autumn 2011. On top of that control, we add either all-sky AMSR-E (these experiments were run for early 2011 when it was still available) or all-sky AMSU-A channel 4 from just two satellites (Metop-A and NOAA-19). In this context, the addition of all-sky

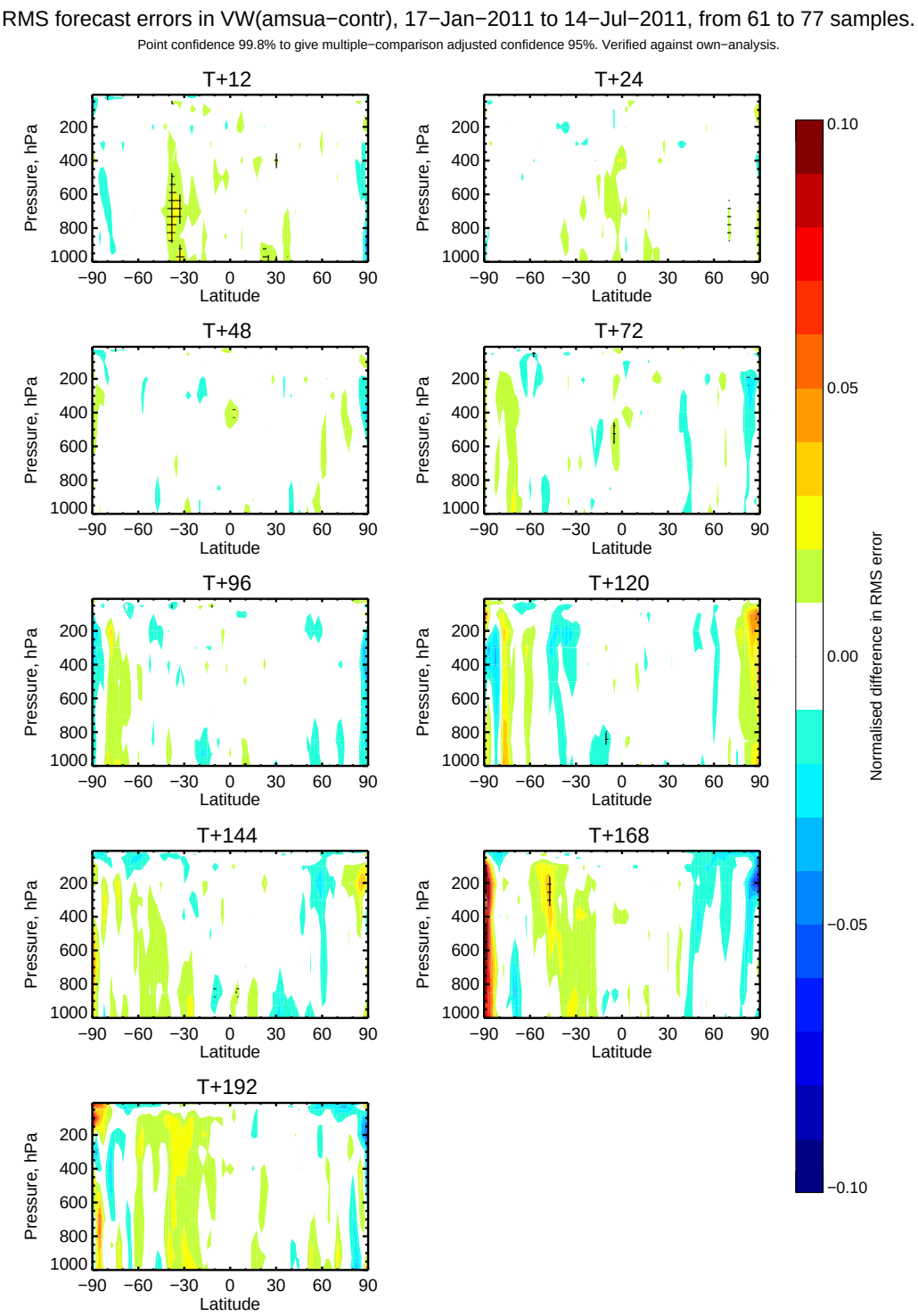

Figure 15: Normalised change in RMS errors in vector wind when AMSU-A channel 4 is assimilated. Blue areas indicate reduced RMS forecast errors and hence improved forecasts; green/yellow/red areas indicate the opposite. Cross hatching indicates a statistically significant change.

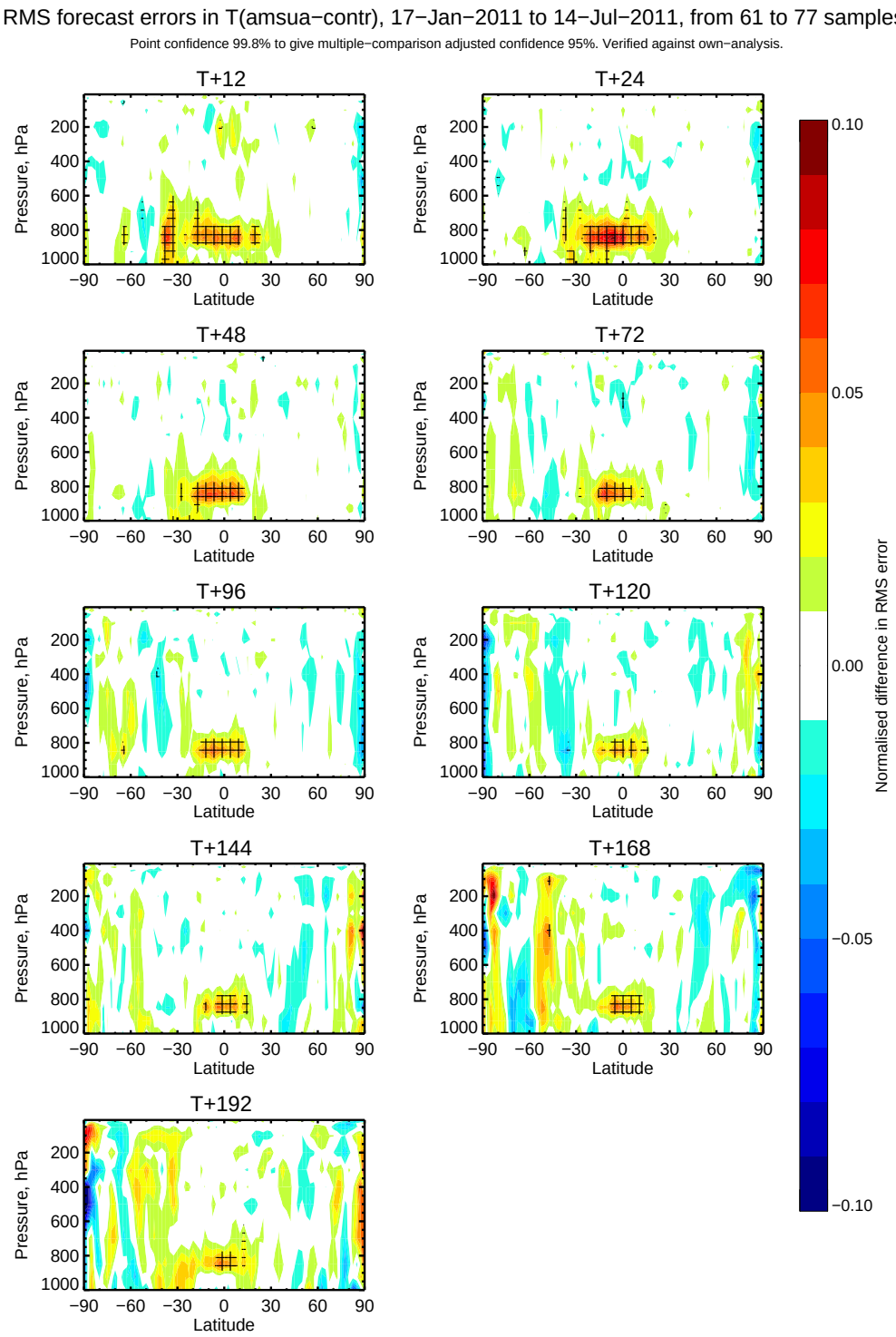

Figure 16: As Fig. 15 but for temperature.

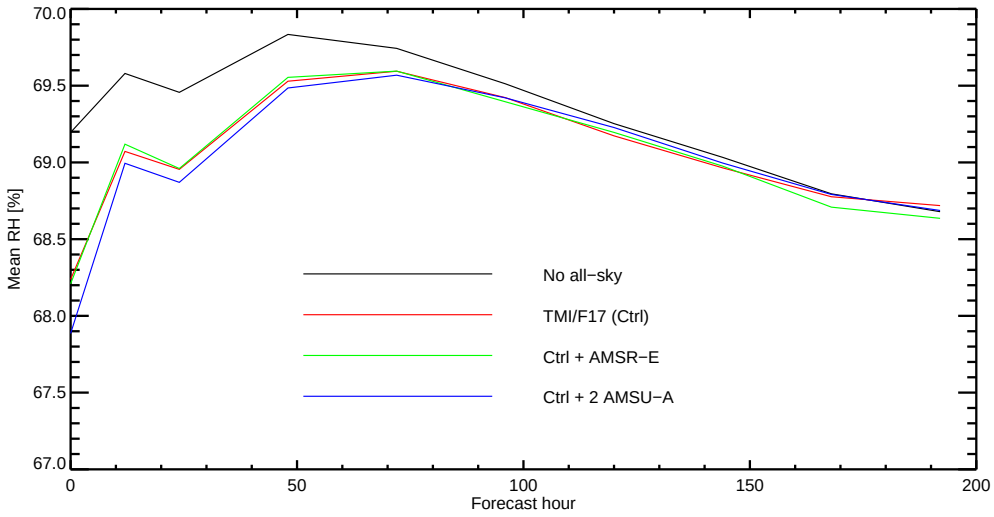

Figure 17: Mean relative humidity in the tropics (20°N to 20°S) at 850 hPa as a function of forecast hour, starting from the analysis (hour 0). Averaging period is 17th January to 5th February 2011. Steps are at 0 h, 12 h, 24 h and every 24 h thereafter

AMSU-A makes a relatively minor change to the temperature and moisture spinup. However, the addition of AMSR-E has even less effect on the spinup.

We can measure the benefits of these various configurations using four observation fit metrics (Fig. 19): AMSU-A channel 5, indicative of mid-tropospheric temperature; HIRS channel 7, indicative of lower tropospheric temperature and WV; and TCWV and LWP estimated from SSMIS F16 brightness temperatures. AMSU-A and HIRS are assimilated; SSMIS F16 is not. The fits have all been normalised so that the first guess fit of the baseline is 100%. The addition of two all-sky imagers is obviously beneficial, bringing improvements of up to 13% in analysed and forecast water vapour and cloud. AMSR-E and AMSU-A channel 4 bring further minor improvements but these are hard to discern from the figure. Experience also shows that such minor differences are not statistically reliable, though it is not easy to compute an error bar for these fits. Figure 20 shows the size of these improvements relative to the control. AMSU-A channel 4 is better than AMSR-E at improving the 'temperature' fit (i.e. AMSU-A channel 5), but otherwise the two configurations are comparable.

4.2.3 Summary

The impact of all-sky AMSU-A channel 4 is more obvious in cloud and water vapour than in temperature. In fact, assimilation of all-sky AMSU-A channel 4 from two satellites has a similar impact to adding a new microwave imager (Fig. 20). All-sky assimilation (whether of AMSU-A or the real imagers, e.g. TMI and SSMIS) causes small tropical spinups in temperature and water vapour at 850 hPa and consequent increases in RMS forecast errors. This issue has been present since the days of the 1D+4D-Var assimilation of cloud-affected microwave imager radiances (Geer et al., 2008), though it was the drying aspect that was most noticeable then. This tropical drying / warming is likely a basic feature of the assimilation system when dealing with moist variables in saturated or near-saturated areas. Geer and Bauer (2010) have already shown that this effect makes no impact on medium-range forecasts and that the change in short-range forecast scores (e.g. Fig. 16) can be considered an artefact of own-analysis verification. Nevertheless, there is still a real issue in the all-sky assimilation that needs to be solved. In this context, the benefit of adding the first two imager-type instruments

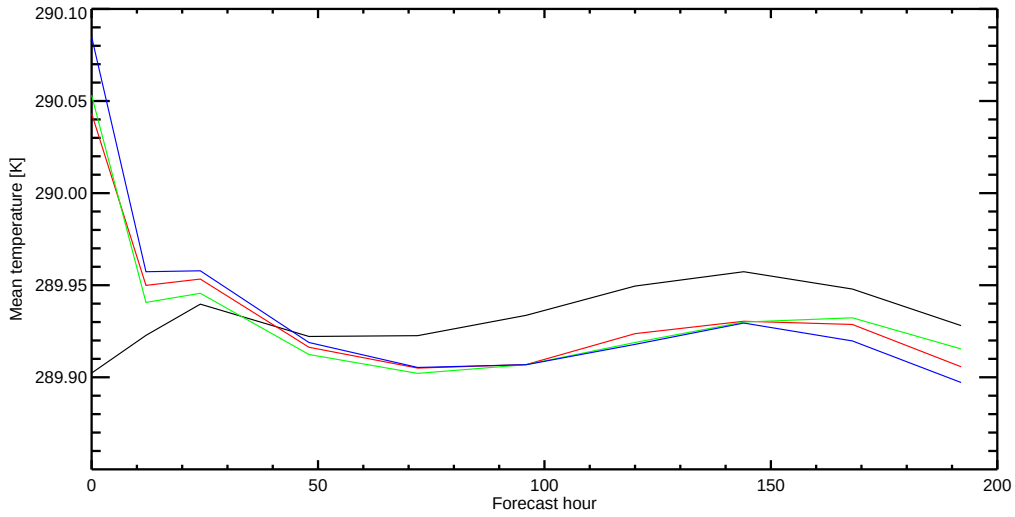

Figure 18: As Fig. 17 but for temperature.

is much clearer than that of adding subsequent ones.

5 Results for channel 5

AMSU-A channel 5 is one of the most important single channels in the observing system in terms of forecast skill (AMSU-A channel 6 may be a little more important, and IASI and AIRS make their influence through weight of numbers.) The clear-sky assimilation of AMSU-A has already benefitted from a decade of careful attention and tuning, including a decrease in prescribed observation error that was beneficial to forecast scores (Bormann et al., 2011b). Hence, channel 5 assimilation will be difficult to improve on, and provides a stern test of the all-sky approach.

Given that channel 5 is operational, it is much harder to do a 'clean' comparison between all-sky and clear-sky approaches for channel 5 than for channel 4. We have not yet been able to achieve a clean experiment; the one presented here suffers a number of defects. It is still worth examining, both to record the subtle but important issues affecting this kind of experiment, but also because we gained insight into what we can expect from all-sky assimilation of temperature channels.

Based on the 37r2 control experiment shown in Tab. 3, an all-sky channel 5 experiment was created. Clear-sky channel 5 was replaced by all-sky over the oceans, following the same geographical range and sea-ice screening criteria, e.g. 90°N to 60°S with sea-ice screened out. Over land, channel 5 continued to be assimilated in the usual way through the clear-sky system. Unfortunately, what initially seemed a simple change introduced numerous differences:

- Thinning strategies were different, so over ocean, all-sky AMSU-A used roughly 250,000 observations per day versus 100,000 for clear-sky AMSU-A channel 5. It is possible that all-sky was over-constraining the temperature because of this;

- As mentioned in Sec. 3.1, in all-sky, we implemented neither the skin temperature sink variable nor the

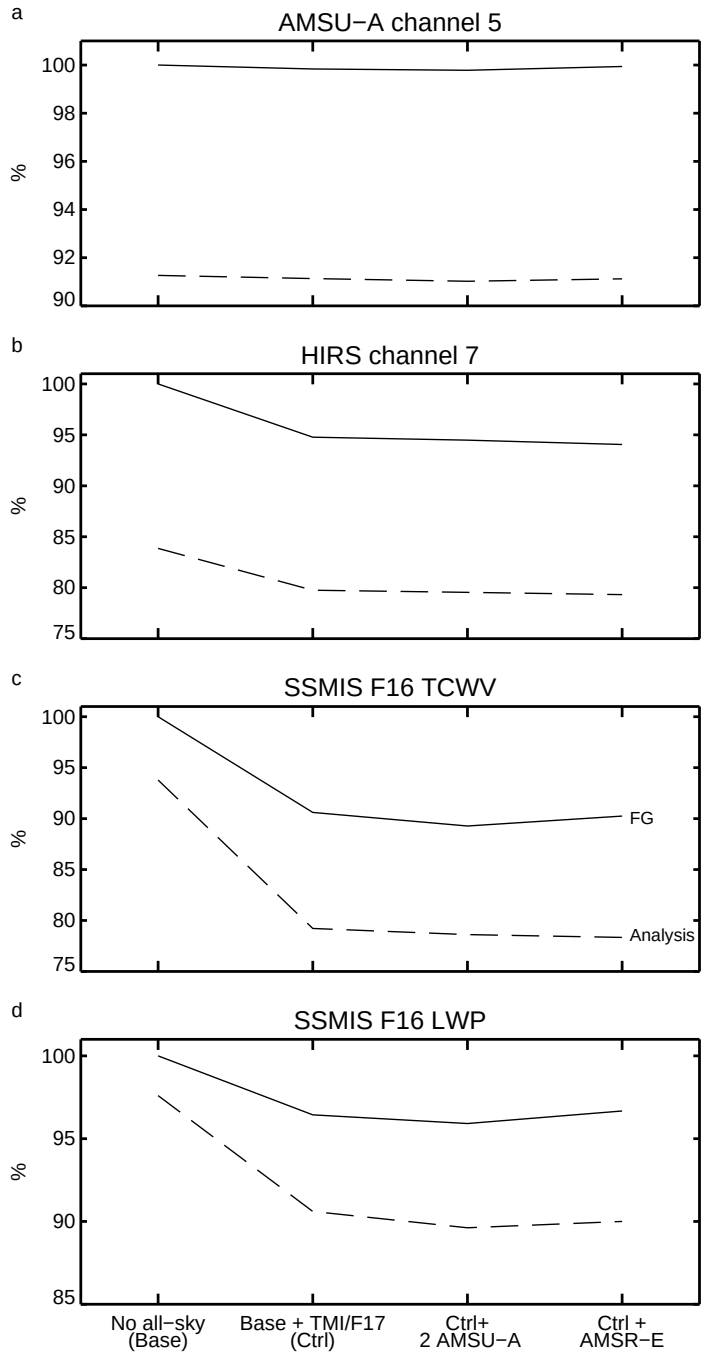

Figure 19: Observation fits, i.e. the standard deviation of FG or analysis departures. These have been normalised by the base experiment's FG departure standard deviation, so that the fit in the base experiment at FG corresponds to 100%. Solid line indicates FG and dashed line analysis. Sample is 17 January to 5 February 2011.

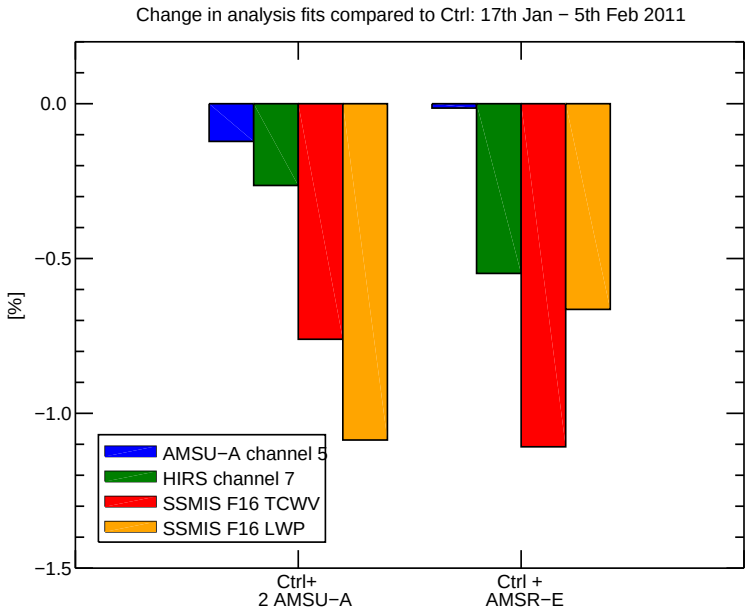

Figure 20: Based on Fig. 19, the change in analysis fit caused by adding either AMSU-A channel 4 or AMSR-E to an otherwise complete operational observing system (the Ctrl experiment). Negative numbers indicate an improved fit.

preferential thinning selection of smaller FG departures. These procedures may make a greater contribution to the quality of clear-sky assimilation than was originally thought;

- A better experiment would have used constant observation errors. The prescribed all-sky errors for channel 5 are between 0.25 K and 0.4 K (Fig. 5c), so except in the very clearest conditions, observation errors are larger in the all-sky assimilation than the 0.28 K used in the clear-sky approach. Given the results of Bormann et al., it would not be surprising if this translated into degradations in forecast scores;

It was found that all-sky assimilation of channel 5 caused an order 1% degradation in fits to temperature-sensitive instruments like sondes (Fig. 21) and IASI (not shown), along with similar size degradations in NH forecast scores, though tropical and SH scores were not affected (Fig. 22). Given the state of development of the clear-sky approach, just matching the quality of the current system would be a good achievement. Nevertheless, we should take a hard look at precisely what we can expect all-sky assimilation to do for the temperature channels.

An initial criticism of the all-sky approach is that it could be reducing the temperature constraint by allowing increments to go into the cloud fields rather than temperature. The channel 5 experiment is not capable of proving this one way or another, but the channel 4 experiments suggest this may be happening (e.g. Fig. 14). Second, there is limited scope for all-sky assimilation to bring more observational coverage, partly because we cannot yet assimilate scattering-affected (e.g. deep convective) areas, but mainly because channel 5 is relatively insensitive to boundary layer cloud and so the 'clear-sky' assimilation already operates in many cloudy areas. In the clear-sky route over ocean, FG departures are computed for AMSU-A channel 3 ignoring cloud and precipitation; where these departures are greater than 3 K the channel 5 observations are considered cloud-affected and are discarded. After this cloud-screening, 80% of observations remain compared to about 96% after the all-sky screening for scattering (these figures are for ocean surfaces only). Hence, all-sky cannot

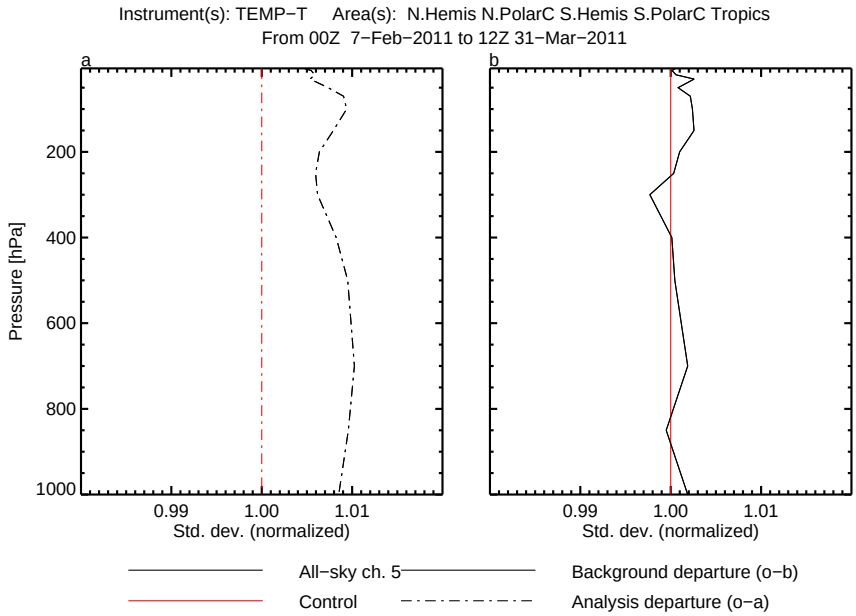

Figure 21: Standard deviation of (a) analysis and (b) FG departures from assimilated radiosonde temperature observations. Standard deviations have been normalised by the control values.

greatly extend the observational coverage. This is in contrast to the experience of the Met Office in their transition to cloudy AMSU-A assimilation (English et al., 2007). This superseded a clear-sky approach that retained only roughly 60% of AMSU-A channel 5 observations after cloud screening. Hence there was much greater scope to expand the observational coverage.

Coverage aside, it would be hoped that all-sky assimilation would help mitigate any problems of undetected liquid water cloud. There must be some residual cloud in the clear-sky data, and the cloud signal would be aliased into the temperature increments. We can compute mean FG departures with and without including hydrometeors in the observation operator (Fig. 23). These departures are computed inside the all-sky approach and include the VarBC bias correction. We apply the standard all-sky quality screening but do not apply any further cloud screening because that would cause a sampling bias and prejudice our comparison (see e.g. Geer et al., 2008; Geer and Bauer, 2011). In this sample, which excludes deep-convective areas but includes other cloudy areas, accounting for hydrometeors in the observation operator reduces biases in NH and SH storm tracks by around 0.05 to 0.15 K. However, it does not eliminate the main geographical patterns of bias apart from in the Southern Ocean. Indeed, it worsens some areas, such as the negative biases in the subtropical stratocumulus regions. Assuming that the first guess hydrometeor fields are not themselves biased, it appears that undetected liquid water cloud is not a major source of bias. Given that the clear-sky assimilation uses a sample where cloud screening has been applied, it is even less likely to be affected by biases relating to undetected cloud. The remaining bias in Fig. 23 has a geophysical pattern but it is not clear where that might come from. SSTs are prescribed from OSTIA analyses that are based on satellite retrievals that may not have as sophisticated an approach to clouds and cloud-screening as the current study, but at the quoted accuracy (around 0.7K, Stark et al., 2007) and with a $\simeq$0.1 atmospheric transmittance in channel 5, this would not be a major factor. There could still be inadequacies in the observation operator, particularly in the emissivity modelling, whose errors are much more important than SST errors over oceans (English, 2008). Equally though, there may be deficiencies in modelled temperature or water vapour fields.

Looking now at the RMS of the FG departures, we can reinforce the argument that undetected clouds are not a

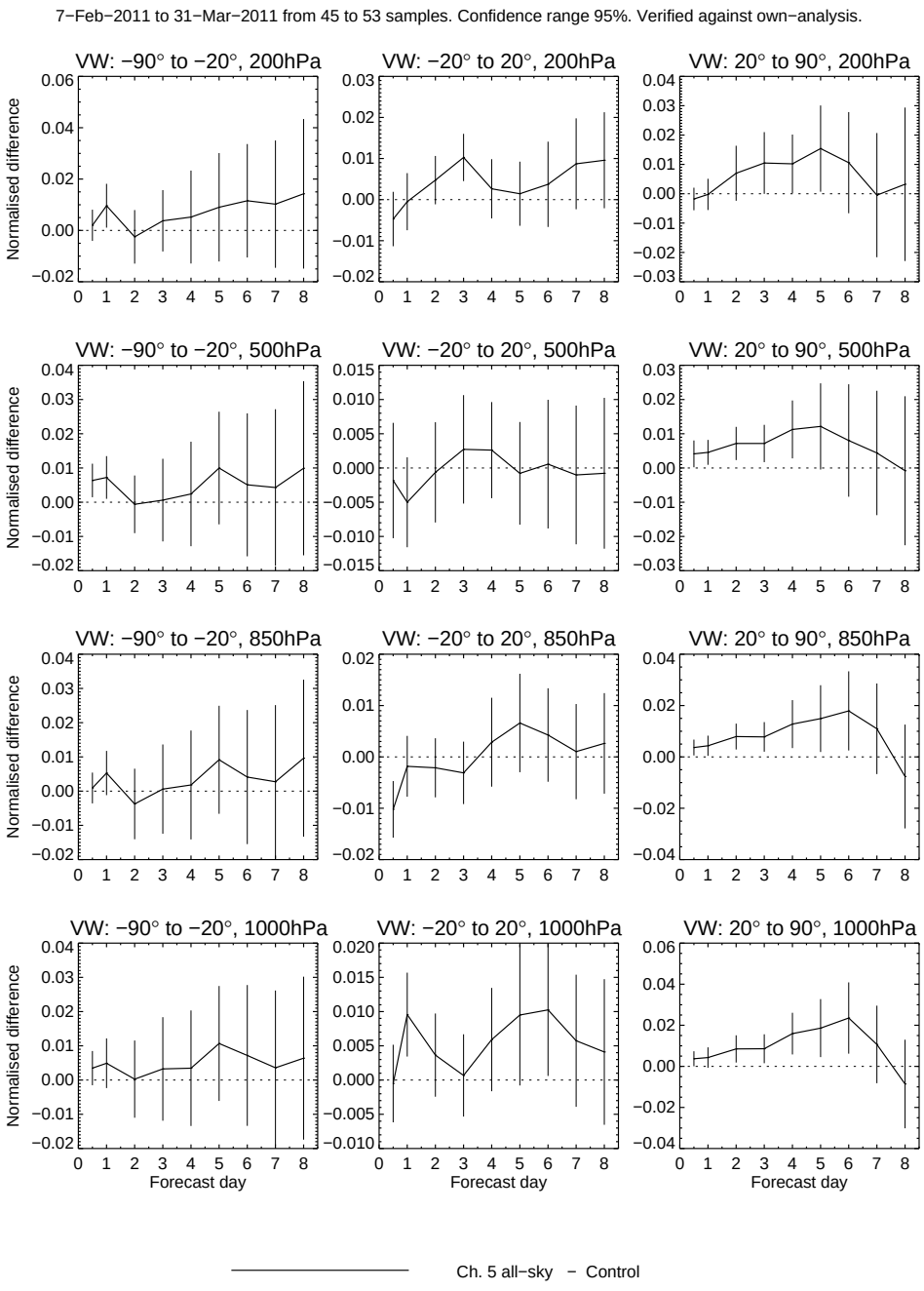

Figure 22: Change in forecast scores coming from assimilating AMSU-A channel 5 through the all-sky route, by comparison to a control where it is assimilated in the clear-sky route. The figure shows the normalised difference in RMS vector wind forecast error between experiment and control, using own-analyses as the reference. Reduced RMS errors indicate better forecasts.

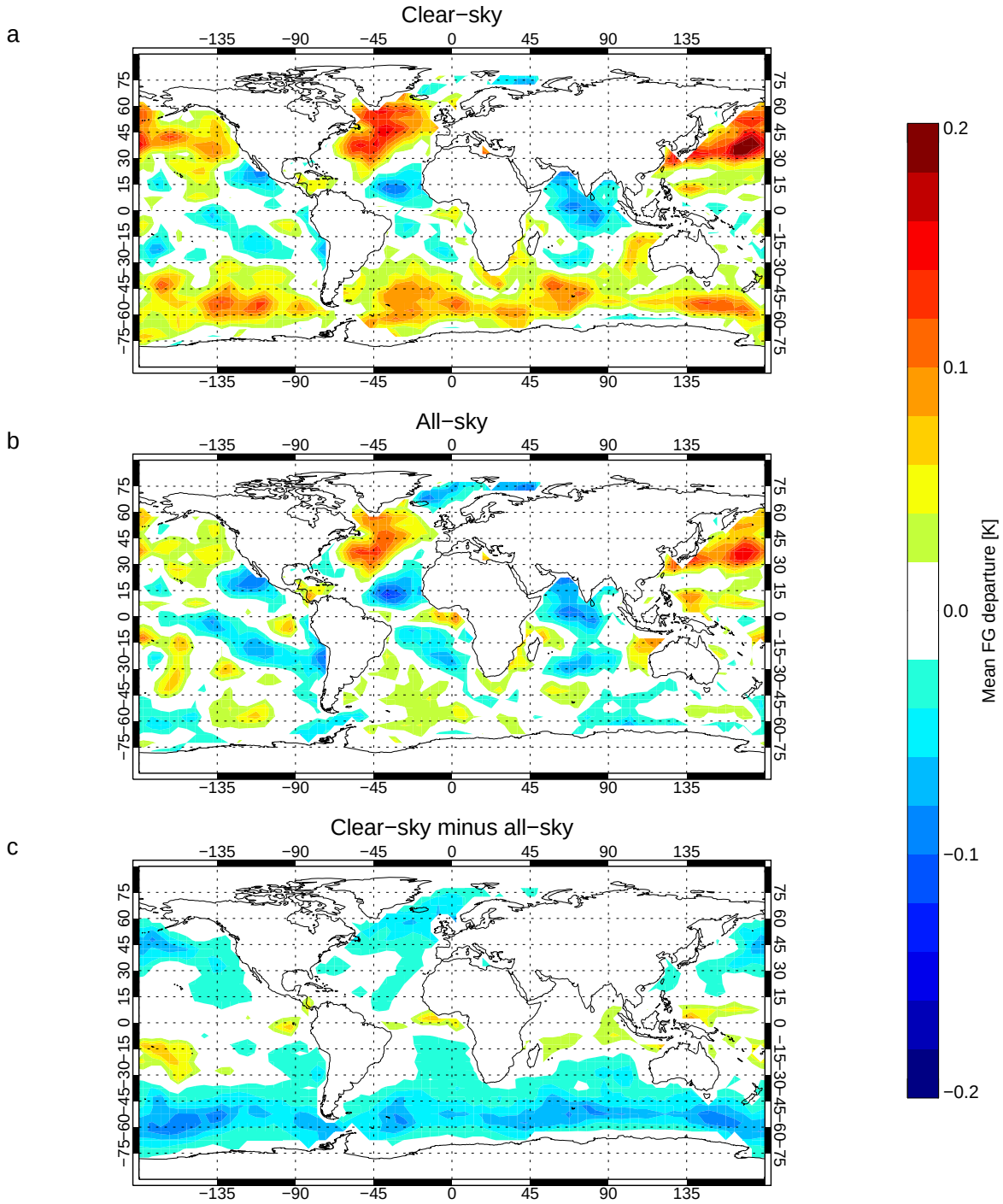

Figure 23: Mean of bias-corrected FG departures in AMSU-A channel 5, binned to a 5° latitude-longitude grid, either (a) ignoring or (b) including cloud and precipitation radiative transfer. Panel (c) shows the difference between the two. The sample is all ocean and sea-ice observations passing the all-sky quality checks, and is based on the period 15 - 28 Feb 2011 (longer periods would make excessive demands on the graphics software). These departures are taken from the control experiment, using the passively-monitored all-sky datastream.

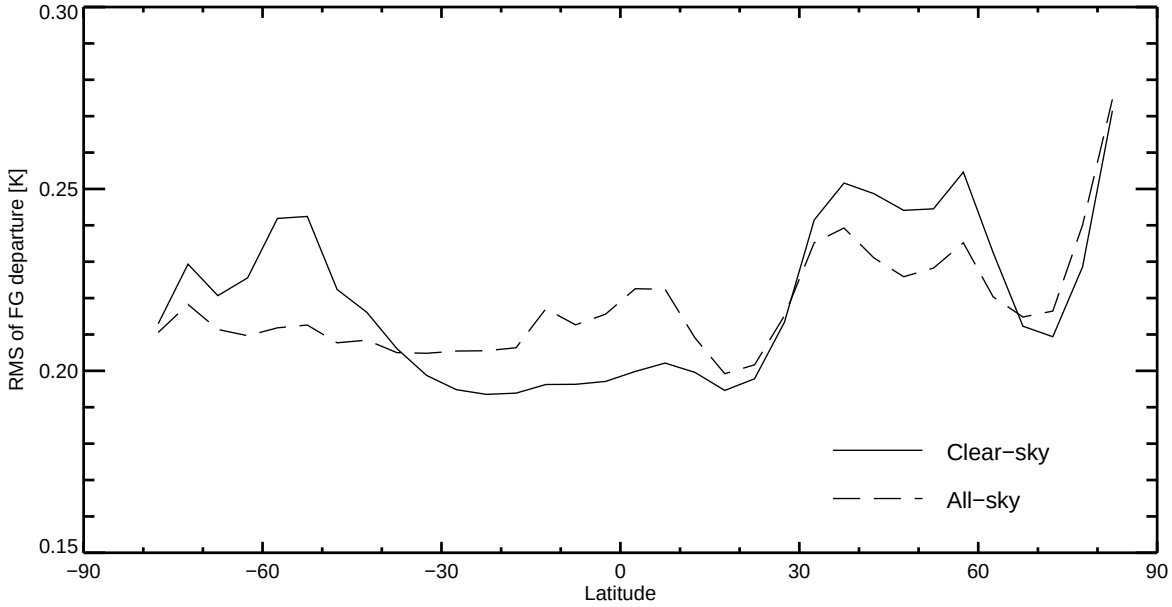

Figure 24: As Fig. 23 but showing the RMS of FG departures in AMSU-A channel 5 binned by latitude, either including (dashed) or ignoring (solid) cloud and precipitation radiative transfer.

very significant error source in clear-sky channel 5 assimilation. Fig. 24 shows the RMS of the FG departures when hydrometeors are either modelled or ignored (using the same sample as Fig. 23, but with zonal bins). In the best case in the SH storm tracks, RMS departures are reduced from 0.24 K to 0.21 K when cloud is correctly modelled. In other latitude bands RMS departures are either unaffected or increased slightly. The tropical increase can partly be explained by the larger negative biases in subtropical stratocumulus regions shown in Fig. 23. However, there may also be a 'double-penalty' problem. The location of convective cloud and precipitation is far less predictable than that of midlatitude frontal cloud (e.g. Ebert et al., 2007). This means that observed and modelled cloud are often in different places and in these situations RMS FG departures will be larger if the model cloud is included in the radiative transfer than if it is ignored.

One other minor problem with the transition to all-sky channel 5 assimilation over ocean was that it had side-effects on the clear-sky channel 5 assimilation over land. Over-ocean observations were no longer contributing to the computation of the clear-sky channel 5 bias correction. In any experimental configuration, most over-land channel 5 data is rejected due to the difficulty of modelling surface emissivities and temperatures, so only a relatively small number of observations are assimilated over land. These remaining observations are not sufficient to maintain a stable bias correction in the clear-sky stream, where the channel 5 bias corrections develop large, unrealistic variations from day to day (the all-sky bias corrections are by contrast quite steady). This could probably be fixed by increasing the effective 'averaging time' in VarBC for these observations, or by moving the over-land observations into the all-sky stream. However, it is also possible that ocean observations actually help maintain the over-land bias correction. This is yet another complex area that needs to be considered more carefully in future experiments.

6 Conclusion

This report has investigated the assimilation of AMSU-A tropospheric temperature channels using the all-sky framework. The focus is on channels 4 and 5, sensitive mainly to lower-tropospheric temperature, hydrometeors (particularly liquid water cloud) and the surface. The radiative transfer of scattering from frozen hydrometeor is not reliable, so the all-sky approach is not applied in situations where scattering is dominant, such as in deep convection. The all-sky framework, previously used for microwave imagers, was adapted for AMSU-A assimilation. The observation error was prescribed using the approach of Geer and Bauer (2011), which assigns larger errors in cloudy and precipitating regions than in clear skies. The 'symmetric' liquid water path (the mean of observation and model) was used as a predictor for observation error. There was also a new term for AMSU-A channels 3 and 4 to describe the cross-scan variation in observation error. This was needed because errors are largest in the central scan positions, where the weighting functions are lower in the atmosphere and there is greater sensitivity to cloud and the surface.

AMSU-A channel 4 was tested in both clear-sky and all-sky configurations, since it is not used operationally in either method. Using the clear-sky approach, channel 4 improves temperature and moisture observation fits at analysis and FG by up to 0.5%, but this does not translate into an improvement in forecast scores. This is probably because lower-tropospheric temperature information is already assimilated over the ocean from AIRS, IASI. Also, the AMSU-A channel 4 weighting function has subtantial overlap with that of channel 5, which is already assimilated. In contrast, the all-sky approach improves fits to microwave imagers by up to 3% at analysis, indicating improved cloud and moisture fields, and there were some significant improvements of around 0.5% (and a smaller number of degradations) in forecast scores. The cloud-sensitivity of AMSU-A channel 4 brings new information to the analysis, even if the temperature information goes largely unused. Hence, on top of the full observing system, adding AMSU-A channel 4 from two satellites brings much the same information as would be provided by adding another microwave imager. However, own-analysis temperature scores in the tropics are degraded because all-sky AMSU-A warms the analyses by 0.05 K at 850 hPa, aggravating an existing temperature and moisture spin-down. The new information brought by AMSU-A channel 4 was not considered sufficient to justify an operational implementation before the spin-down problem has been fixed. In contrast, though the existing all-sky microwave imager assimilation (using TMI and SSMIS radiances) is affected by a similar issue, the 0.15 K mean change in tropical 850hPa temperature is more than compensated by an up to 13% improvement in water vapour and cloud fields.

AMSU-A channel 5 is one of the most important data sources in the observing system. Moving this channel out of the clear-sky approach (where it is already operationally assimilated) and into the all-sky stream over oceans (for latitudes between 90°N and 60°S) caused degradations of up to 1% in observation fits and scores. However, this initial experiment was not well designed, and the impact of all-sky assimilation was combined with many other implementation differences, such as changes in the prescribed observation error, the number of observations, thinning, observation coverage, VarBC, and the use (or not) of a skin temperature sink variable. It should at least be possible to replicate the quality of the clear-sky assimilation of channel 5 in the future, but it will require further development, and we will need to design experiments that better isolate the technical and scientific changes involved. Nonetheless, we have highlighted a number of issues that may make it difficult to improve on clear-sky assimilation:

- All-sky assimilation could actually reduce the constraint on temperature by allowing increments to go into the cloud fields;
- There is relatively little scope to extend the observational coverage in AMSU-A channels 5 and 6 beyond what is available in the 'clear-sky' approach: operationally only 20% of these observations are removed by cloud screening.

- Untreated liquid water cloud is a minor part of the error budget for clear-sky channel 5 assimilation. Even when liquid water cloud is properly modelled using the all-sky approach, the geographical patterns of bias are mostly unaffected, and globally the RMS of FG departures is not improved;
- The 'double-penalty' problem can increase the error budget in all-sky assimilation (compared to clear-sky), particularly in the tropics;
- The all-sky technique suffers ongoing issues with water vapour and temperature spinup in the tropics, likely to do with the data assimilation and the water vapour control variable.

We still hope to make further developments in this area. It would be good to test AMSU-A channels 1, 2, 3, 4 and 15 as a backup for water vapour and cloud assimilation in a future 'no microwave imager' scenario. Work is ongoing to improve the radiative transfer of scattering from frozen particles, which may eventually allow the use of AMSU-A channels 4, 5 and 6 in deep-convective areas. We can also try to better distinguish the truly scattering situations from those where the brightness temperature is depressed by the upward shift of the weighting function in heavy rain and cloud. Use of a scattering index rather than the 'cloud delta' (Eq. 1) may help make this distinction. Finally, AMSU-A channel 3 may be useable for temperature away from nadir, where it has a higher atmospheric information content.

There is also the possibility to include more cloud and precipitation information from microwave humidity sounding channels, e.g. on MHS and AMSU-B. Perhaps with sufficient constraint of cloud and precipitation from these and the imager-type channels, the temperature increments from sounding channels can be better constrained.

Acknowledgements

Alan Geer was funded by EUMETSAT via the fellowship programme and NWP-SAF. Niels Bormann provided a lot of assistance on AMSU-A assimilation and in reviewing the memo. Jean-Nöel Thépaut, Philippe Lopez, Bill Bell, Tony McNally, Anne Fouilloux, Deborah Salmond, Sabatino DiMichele, Blazej Krzeminski, Reima Eresmaa, Mohamed Dahoui, Jan Haseler, Gabor Radnoti and Paul Dando are also thanked for their help in this work.

A Approximate LWP retrieval for AMSU-A

In the all-sky assimilation of microwave imagers, the approximate Karstens et al. (1994) liquid water path (LWP) retrieval is widely used:

$$\mathrm{LWP} = c_1 + c_2 \ln(280 - T_{22V}) + c_3 \ln(280 - T_{37V}) \tag{7}$$

The coefficients c_1 to c_3 are derived by linear regression; T_{22V} and T_{37V} are the brightness temperatures of the SSM/I 22 GHz and 37 GHz vertically polarised channels. In rough physical terms, this can be seen as estimating the effect of atmospheric water vapour using the 22 GHz channel, and then retrieving the additional cloud signal using the cloud-sensitive 37 GHz channel. AMSU-A provides 22 GHz and 31 GHz channels, so a similar retrieval technique can be applied, but the variation of zenith angle, polarisation and surface emissivity as a function of scan position must be accounted for. One option would be to derive a different set of coefficients for each scan position, but this would be cumbersome. Instead, the formulation can be extended to include the dependence on zenith angle and surface effects.

For microwave window channels, the brightness temperature T_ν at frequency ν can be approximated (Grody et al., 1980) from the exact radiative transfer equation as:

$$T_\nu = T_0 \left(1 - \tau_\nu^2 (1 - \varepsilon_S)\right) \tag{8}$$

Here, T_0 is an effective atmospheric temperature, which is a mean temperature weighted according to the radiative influence of each atmospheric layer, τ_ν is the surface to space transmittance and ε_S the surface emissivity. Two major assumptions have been made: that the effective atmospheric temperature is equivalent for both upwelling and downwelling radiation, and that the surface temperature is similar to the effective atmospheric temperature. These assumptions can only really be justified for imager channels where the atmospheric emission normally comes from the lowest layers of the atmosphere. Also, surface reflection has been assumed specular though for more quantitative purposes this does not hold (e.g. Petty and Katsaros, 1994).

The surface-to-space transmittance along a path with zenith angle θ can be written:

$$\tau_\nu = \exp\left(-k_\nu^W \left(\frac{\mathrm{TCWV}}{\cos\theta}\right) - k_\nu^L \left(\frac{\mathrm{LWP}}{\cos\theta}\right)\right), \tag{9}$$

This depends on the vertically integrated amounts of water vapour (TCWV) and cloud liquid water (LWP) and the relevant mass absorption coefficients k_ν^W and k_ν^L. This ignores other absorber (such as oxygen, precipitation and cloud ice), scattering effects, and any temperature or pressure dependence of the absorption coefficients.

Given that AMSU-A observes brightness temperatures at 22 GHz and 31 GHz (T_{22} and T_{31}), we can write Eqs. 8 and 9 for each of the two frequencies, then eliminate TCWV in order to solve for LWP. This gives:

$$\mathrm{LWP} = \cos\theta \left(a_1 \left(\ln(T_0) + \ln(1 - \varepsilon_S)\right) + a_2 \ln(T_0 - T_{22}) + a_3 \ln(T_0 - T_{31})\right) \tag{10}$$

Here the coefficients a_1 to a_3 are slightly complicated functions of the absorption coefficients for water vapour and liquid at the two frequencies (k_{22}^W, k_{22}^L, k_{31}^W and k_{31}^L). However they do not depend on anything else, so they can be treated as constants. There is an explicit dependence on zenith angle via $cos\theta$ and an implicit dependence on zenith angle and polarisation via the surface emissivity ε_S. In practice, the coefficients are derived from fits to simulated observations, rather than directly from the radiative properties of cloud and water vapour, as might be implied by Eqs. 8 and 9. Equation 10 reduces to the Karstens et al. (1994) retrieval (Eq. 7) if the zenith angle and polarisation are constant.

Starting from the Grody et al. (2001) coefficients, which are already used as part of an emissivity retrieval in the clear-sky assimilation, but adding a slightly improved zenith angle dependence, the following retrieval was developed:

$$\mathrm{LWP} = \cos\theta \left(8.24 - (2.539 - 1.744\cos\theta)\cos\theta + 0.754 ln(285 - T_{22}) - 2.265 ln(285 - T_{31})\right) \tag{11}$$

The emissivity term $a_1(ln(1 - \varepsilon_S))$ has been parametrised in the form $(a + bcos\theta)cos\theta$, and is computed (using linear regression) by trying to make cross-scan variations in LWP as small as possible. To test the retrieval, it was applied to 10 days' brightness temperatures simulated from the model FG profiles at AMSU-A locations. Figure 25 compares the retrievals to the 'true' LWP in the FG. There is a considerable amount of scatter around the 1:1 line, but this is to be expected given the assumptions that go into our retrieval. It is still adequate for use in the parametrisation of observation error.

B Acronyms

Here are some acronyms that are not defined in the main body of the text:

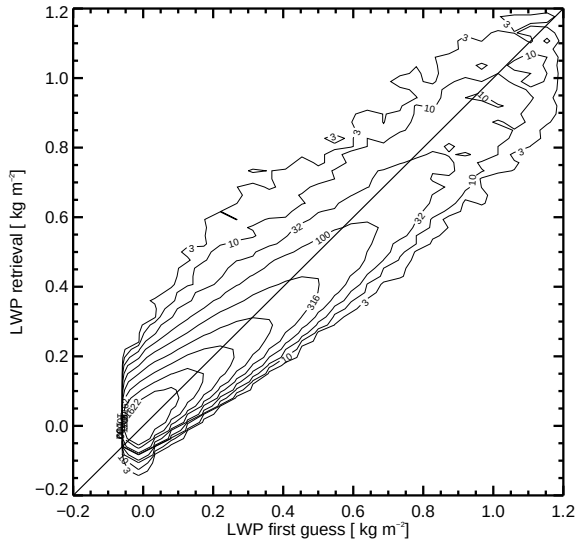

Figure 25: Scatter-plot of retrieved versus simulated LWP, with the 1:1 line superimposed. Density of points is given by logarithmic contours. Sample is 10 days of simulated profiles at AMSU-A locations. Correlation coefficient is 92.7%.

AIRS – Advanced Infrared Sounder
AMSR-E – Advanced Microwave Sounder Radiometer for EOS
EOS – NASA Earth Observing System
EUMETSAT – European Organisation for the Exploitation of Meteorological Satellites
OSTIA – Operational Sea Surface Temperature and Sea Ice Analysis
HIRS – High Resolution Infrared Radiation Sounder
IASI – Infrared Atmospheric Sounding Interferometer
ITCZ – Inter-tropical convergence zone
MHS – Microwave Humidity Sounder
NOAA – National Oceanic and Atmospheric Administration
QuikSCAT – Quick Scatterometer
RTTOV-SCATT – Radiative Transfer for TOVS - Scattering
SSM/I – Special Sensor Microwave Imager
SSMIS – Special Sensor Microwave Imager / Sounder
TIROS – Television Infrared Observation Satellite Program
TMI – TRMM Microwave Imager
TOVS – TIROS Operational Vertical Sounder
TRMM – Tropical Rainfall Measuring Mission

References

Baker, N. L., T. F. Hogan, W. F. Campbell, R. L. Pauley, and S. D. Swadley (2005). The impact of AMSU-A radiance assimilation in the U.S. Navy's opertional global atmospheric prediction system (NOGAPS). *Naval Research Laboratory report NRL/MR/7530--05-8836.*

Bauer, P., T. Auligné, W. Bell, A. Geer, V. Guidard, S. Heillette, M. Kazumori, M.-J. Kim, E. J.-C. Liu, A. P.

McNally, B. Macpherson, K. Okamoto, R. Renshaw, and L.-P. Riishøjgaard (2011). Satellite cloud and precipitation assimilation at operational NWP centres. *Quart. J. Roy. Meteorol. Soc.*, doi:10.1002/qj.905.

Bauer, P., A. J. Geer, P. Lopez, and D. Salmond (2010). Direct 4D-Var assimilation of all-sky radiances: Part I. Implementation. *Quart. J. Roy. Meteorol. Soc. 136*, 1868–1885.

Bauer, P., E. Moreau, F. Chevallier, and U. O'Keeffe (2006). Multiple-scattering microwave radiative transfer for data assimilation applications. *Quart. J. Roy. Meteorol. Soc. 132*, 1259–1281.

Bennartz, R. (2000). Optimal convolution of AMSU-B to AMSU-A. *J. Atmos. Ocean Tech. 17*, 1215–1225.

Bormann, N. (2008). Modification of AMSU-A quality control to reintroduce tropospheric channels from NOAA-16 and Aqua. *ECMWF Research Department Internal Memorandum R48.3/NB/0887*.

Bormann, N., A. Geer, and P. Bauer (2011a). Estimates of observation error characteristics in clear and cloudy regions for microwave imager radiances from NWP. *Quart. J. Roy. Meteorol. Soc. 137*, 2014–2023.

Bormann, N., J.-N. Thépaut, and P. Bauer (2011b). Increased weight for AMSU-A in 37R1. *ECMWF Research Department Internal Memorandum R48.3/NB/1118*.

Cardinali, C. and F. Prates (2011). Performance measurement with advanced diagnostic tools of all-sky microwave imager radiances in 4D-Var. *Quart. J. Roy. Meteorol. Soc. 137*, 2038–2046.

Dee, D. (2004). Variational bias correction of radiance data in the ECMWF system. In *ECMWF workshop proceedings: Assimilation of high spectral resolution sounders in NWP, 28 June – 1 July, 2004*, pp. 97–112. Eur. Cent. for Med. Range Weather Forecasts, Reading, UK, available from http://www.ecmwf.int.

Derber, J. C. and W.-S. Wu (1998). The use of TOVS cloud-cleared radiances in the NCEP SSI analysis system. *Mon. Weath. Rev. 126*, 2287–2299.

Ebert, E. E., J. E. Janowiak, and C. Kidd (2007). Comparison of near-real-time precipitation estimates from satellite observations and numerical models. *Bull. Am. Met. Soc. 88*, 47–64.

English, S., U. O'Keeffe, and M. Sharpe (2007). Assimilation of cloudy AMSU-A microwave radiances in 4D-VAR. In *15th International TOVS Study Conference, Maratea, Italy, 4-10 October 2006 (proceedings)*, pp. 447–454. University of Wisconsin-Madison, Space Science and Engineering Center, Cooperative Institute for Meteorological Satellite Studies (CIMSS), Madison, WI, available from http://library.ssec.wisc.edu/research_Resources/publications/index?selSeries=tovs.

English, S. J. (2008). The importance of accurate skin temperature in assimilating radiances from satellite sounding instruments. *Quart. J. Roy. Meteorol. Soc. 126*, 2911–2931.

English, S. J., R. J. Renshaw, P. C. Dibben, A. J. Smith, P. J. Rayer, C. Poulsen, F. W. Saunders, and J. R. Eyre (2000). A comparison of the impact of TOVS and ATOVS satellite sounding data on the accuracy of numerical weather forecasts. *IEEE Trans. Geosci. Remote Sens. 46*, 403–408.

Geer, A. J. and P. Bauer (2010). Enhanced use of all-sky microwave observations sensitive to water vapour, cloud and precipitation. *Published simultaneously as ECMWF Technical Memoranda 620 and ECMWF/EUMETSAT fellowship reports 20*.

Geer, A. J. and P. Bauer (2011). Observation errors in all-sky data assimilation. *Quart. J. Roy. Meteorol. Soc. 137*, 2024–2037.

Geer, A. J., P. Bauer, and P. Lopez (2008). Lessons learnt from the operational 1D+4D-Var assimilation of rain- and cloud-affected SSM/I observations at ECMWF. *Quart. J. Roy. Meteorol. Soc. 134*, 1513–1525.

Geer, A. J., P. Bauer, and P. Lopez (2010). Direct 4D-Var assimilation of all-sky radiances: Part II. Assessment. *Quart. J. Roy. Meteorol. Soc. 136*, 1886–1905.

Geer, A. J., P. Bauer, and C. W. O'Dell (2009). A revised cloud overlap scheme for fast microwave radiative transfer. *J. App. Meteor. Clim. 48*, 2257–2270.

Geer, A. J., R. Forbes, P. Bauer, and F. Baordo (2011). Big temperature increments in the 37r3 esuite coming from all-sky observations in the southern winter. *ECMWF Research Department Internal Memorandum R48.3/AG/11110*.

Grody, N., A. Gruber, and W. Shen (1980). Atmospheric water content over the tropical Pacific derived from the Nimbus-6 scanning microwave spectrometer. *J. App. Meteorol. 19*, 986–996.

Grody, N., J. Zhao, R. Ferraro, F. Weng, and R. Boers (2001). Determiniation of precipitatable water and cloud liqid water over oceans from the NOAA 15 advanced microwave sounding unit. *J. Geophys. Res. 106*, 2943 – 2953.

Haseler, J. (2004). Early-delivery suite. *ECMWF Tech. Memo., 454, available from http://www.ecmwf.int*.

Ishibashi, T. (2011). Cloudy radiance assimilation with extension of control variables in 4D-Var. In *WMO WGNE blue book, available from http://collaboration.cmc.ec.gc.ca/science/wgne/*.

Karstens, U., C. Simmer, and E. Ruprecht (1994). Remote sensing of cloud liquid water. *Meteorol. Atmos. Phys. 54*, 157–171.

Klein, S. A., R. B. McCoy, H. Morrison, A. S. Ackerman, A. Avramov, G. de Boer, M. Chen, J. N. S. Cole, A. D. Del Genio, M. Falk, M. J. Foster, A. Fridlind, J.-C. Golaz, T. Hashino, J. Y. Harrington, C. Hoose, M. F. Khairoutdinov, V. E. Larson, X. Liu, Y. Luo, G. M. McFarquhar, S. Menon, R. A. J. Neggers, S. Park, M. R. Poellot, J. M. Schmidt, I. Sednev, B. J. Shipway, M. D. Shupe, D. A. Spangenberg, Y. C. Sud, D. D. Turner, D. E. Veron, K. von Salzen, G. K. Walker, Z. Wang, A. B. Wolf, S. Xie, K.-M. Xu, F. Yang, and G. Zhang (2009). Intercomparison of model simulations of mixed-phase clouds observed during the ARM Mixed-Phase Arctic Cloud Experiment. I: single-layer cloud. *Quart. J. Roy. Meteorol. Soc. 135*, 979–1002.

Kulie, M. S., R. Bennartz, T. J. Greenwald, Y. Chen, and F. Weng (2010). Uncertainties in microwave properties of frozen precipitation: implications for remote sensing and data assimilation. *J. Atmos. Sci. 67*, 3471–3487.

Petty, G. and W. Huang (2010). Microwave backscatter and extinction by soft ice spheres and complex snow aggregates. *J. Atmos. Sci. 67*, 769–787.

Petty, G. and K. Katsaros (1990). Precipitation observed over the south China sea by the Nimbus-7 scanning multichannel microwave radiometer during winter MONEX. *J. App. Meteorol. 29*, 273–287.

Petty, G. W. and K. B. Katsaros (1994). The response of the SSM/I to the marine environment. Part II: A parameterization of the effect of the sea surface slope distribution on emission and reflection. *J. Atmos. Ocean Tech. 11*, 617–628.

Robel, J. (2009). NOAA KLM user's guide (February 2009 revision). *Available from http://www.ncdc.noaa.gov/oa/pod-guide/ncdc/docs/intro.htm*.

Stark, J. D., C. J. Donlon, M. J. Martin, and M. E. McCulloch (2007). OSTIA: An operational, high resolution, real time, global sea surface temperature analysis system. In *Oceans '07 IEEE Aberdeen: Marine challenges: coastline to deep sea, Aberdeen, Scotland*. IEEE.